

710 ASD  
LAS-TR-207-5

March 1962

7238  
AFOSR-2432

AF 49 (638) 1033

EXPERIMENTAL INVESTIGATIONS OF TRANSPORT PROPERTIES  
OF PARTIALLY IONIZED GASES

P. J. Dickerman

FINAL REPORT

**DISTRIBUTION STATEMENT A**  
Approved for Public Release  
Distribution Unlimited

Prepared for  
Air Force Office of Scientific Research  
Office of Aerospace Research  
Contract No. AF 49(638)-1033  
Project No. 9781, Task No. 37713

THE UNIVERSITY OF CHICAGO  
LABORATORIES FOR APPLIED SCIENCES  
CHICAGO 37, ILLINOIS

Reproduced From  
Best Available Copy

Copies Furnished to DTIC  
Reproduced From  
Bound Original

20020715 180

## NOTICES

When Government drawings, specifications, or other data are used for any purpose other than in connection with a definitely related Government procurement operation, the United States Government thereby incurs no responsibility nor any obligation whatsoever; and the fact that the Government may have formulated, furnished, or in any way supplied the said drawings, specifications, or other data, is not to be regarded by implication or otherwise as in any manner licensing the holder or any other person or corporation, or conveying any rights or permission to manufacture, use, or sell any patented invention that may in any way be related thereto.

Qualified requesters may obtain copies of this report from the Armed Services Technical Information Agency, (ASTIA), Arlington Hall Station, Arlington 12, Virginia.

This report has been released to the Office of Technical Services, U. S. Department of Commerce, Washington 25, D. C., for sale to the general public.

## FOREWORD

This is the first annual report, covering the period 15 February 1961 to 15 February 1962, on LAS Task 207, "Research on Experimental Investigations of Transport Properties of Partially Ionized Gases." This program is conducted by the Laboratories for Applied Sciences (LAS) of the University of Chicago for the Air Force Office of Scientific Research under Contract No. AF 49(638)-1033.

University of Chicago personnel who participated in the work covered by this report include: B. P. Alpiner, R. W. Deniel, P. J. Dickerman, H. Halle, and J. R. Hoenig.

## ABSTRACT

Recent advances in electric arc research and development allow stable high-temperature environments to be obtained over extended periods of time in the laboratory. By making use of the known relationships between temperature and conductivity in such arc discharges and by experimentally measuring the current density, electron density, and temperature, the effective cross section of atoms which impede the electron flow can be determined. Thus, atom-electron collision cross sections can now be measured in the interesting energy range of 1 to 2 ev, lower than heretofore possible using conventional beam apparatus. Techniques involved in making the necessary spectroscopic and electrical measurements are given, and results obtained for three gases (argon, helium, and nitrogen) are presented. These results are then used to determine several of the transport properties for these partially ionized gases.

## TABLE OF CONTENTS

<u>Section</u>	<u>Page</u>
1. INTRODUCTION . . . . .	1
2. DISCUSSION . . . . .	2
2.1 Previous Work . . . . .	2
2.2 Cross-Section Determinations Using the Electric Arc. . . . .	3
2.3 Experimental Preparations. . . . .	9
2.4 Preliminary Calculations . . . . .	12
2.5 General Comments on Spectroscopic Temperature Measurements . . . . .	25
2.6 Spectroscopic Temperature Measurements . . . . .	28
2.6.1 Argon . . . . .	28
2.6.2 Helium. . . . .	31
2.6.3 Nitrogen . . . . .	34
2.7 Spectral Line Shapes in Argon . . . . .	36
2.8 Electric Field Determinations . . . . .	38
2.9 Radial Current Density Distributions . . . . .	38
3. RESULTS . . . . .	45
3.1 Cross Sections . . . . .	45
3.2 Transport Properties . . . . .	52
4. BIBLIOGRAPHY . . . . .	58

## LIST OF ILLUSTRATIONS

<u>Figure</u>	<u>Page</u>
1. Low-Energy Collision Probabilities in Hydrogen. . . . .	4
2. Schematic Diagram of the Experimental Arc Chamber . . . . .	8
3. Photograph of the Arc Operating at 50 Amperes in Argon at a Length of 1/2 inch . . . . .	13
4. Photograph of Arc Chamber and Associated Equipment. . . . .	14
5. Voltage-Current Characteristics for 3/8-inch Arc Using: (a) argon; (b) helium; (c) 66% argon, 34% nitrogen. . . . .	15
6. Particle Densities for an Atmospheric Pressure Argon Plasma . . . . .	17
7. Particle Densities for an Atmospheric Pressure Helium Plasma . . . . .	18
8. Particle Densities for an Atmospheric Pressure Nitrogen Plasma. . . . .	19
9. Ion-Electron Cross Sections for Argon at Atmospheric Pressure . . . . .	22
10. Ion-Electron Cross Sections for Helium at Atmospheric Pressure . . . . .	23
11. Ion-Electron Cross Sections for Nitrogen at Atmospheric Pressure . . . . .	24
12. Calculated Intensity-Temperature Distribution of the Atomic $\lambda 8264$ Spectral Line in Argon . . . . .	30
13. Temperature vs. Radius in a 270-ampere Argon Arc Above Anode Surface . . . . .	32

# LIST OF ILLUSTRATIONS (cont'd)

<u>Figure</u>		<u>Page</u>
14.	Temperature vs. Radius in a 350-ampere 34% Nitrogen, 66% Argon Arc Above Anode Surface . . . . .	35
15.	Profile of the $\lambda 8115$ Line in an Argon Arc at 200 Amperes .	37
16.	Arc Voltage vs. Length for 270 Amperes in Argon . . . . .	39
17.	Arc Voltage vs. Length for 230 Amperes in Helium . . . . .	40
18.	Arc Voltage vs. Length for 350 Amperes in 66% Argon, 34% Nitrogen . . . . .	41
19.	Schematic of the Current Probe-Anode . . . . .	42
20a.	Circuitry Used with Current Probe-Anode in Argon and Helium . . . . .	44
20b.	Circuitry Used with Current Probe-Anode in Nitrogen-Argon Mixture . . . . .	44
21.	Current Density vs. Arc Radius in an Argon Arc at 270 Amperes . . . . .	46
22.	Current Density vs. Arc Radius in Helium Arc at 230 Amps .	47
23.	Current Density vs. Arc Radius in the Argon-Nitrogen Arc at 350 Amperes . . . . .	48
24.	Atom-Electron Collision Cross Sections in Argon. . . . .	50
25.	Atom-Electron Collision Cross Sections in Nitrogen . . . . .	51
26.	Electrical Conductivity vs. Temperature for Argon . . . . .	56
27.	Electrical Conductivity vs. Temperature for Nitrogen. . . . .	57

## LIST OF TABLES

<u>Table</u>		<u>Page</u>
1	Values of $\alpha_{ij}$ Used to Transform Observed Intensities to Radial Intensities . . . . .	27
2	Viscosities for Argon and Nitrogen : . . . . .	55



## 1. INTRODUCTION

In considering the rates of certain physical processes and in order to understand many of the important aspects of hydrodynamics, magnetohydrodynamics, and plasma physics, it is necessary to discuss the transport of matter, energy, momentum, and electrical charge by atomic systems. The transport of matter is described by various diffusion coefficients, the transport of energy by the thermal conductivity, the transport of momentum by the viscosity, and the transport of electrical charge by the electrical conductivity. These four quantities (diffusion coefficients, thermal conductivity, viscosity, and electrical conductivity) are thus known as the transport properties.

The fundamental atomic parameters upon which these transport properties depend are the collision cross sections. These cross sections, of course, depend upon particle velocity, or macroscopically speaking, upon the gas temperature. Therefore, measurements must be performed on a system which is precisely within the energy range of interest. Since this work was motivated by the need for data at energies below 2 ev (re-entry conditions, certain astrophysical conditions, shock and detonation wave energies), a new experimental technique using a stable electric arc discharge was employed. It should be noted here that cross-section measurements have been made for many elements in the past using one or another of several beam techniques. However, all of these methods become insensitive below a few volts, necessitating a different experimental approach for the above-mentioned energy range.

It was not the purpose of the present work to generally develop arc technology and experimental techniques, although to be sure several new procedures were found in the course of the program, but rather to

make use of existing knowledge and apply it to the problem of measuring cross sections. The principal difference between the arc and beam methods is that measurements of an arc discharge provide an "effective" cross section (velocities averaged over some distribution), whereas a beam technique yields data for a unique collision velocity. A considerable amount of work [1, 2, 3]\*, however, has shown that local thermodynamic equilibrium (LTE) prevails for arcs run at atmospheric pressure and at temperatures less than 10 ev, since for this condition excitation and de-excitation and ionization and recombination are mainly caused by electron collisions. Thus one is assured that the velocity distribution is maxwellian and that the data obtained here are sufficiently general to be safely applied to other systems with appropriate energies and densities.

## 2. DISCUSSION

### 2.1 PREVIOUS WORK

The problem of determining cross sections for atom-electron collisions is one that had received considerable attention in the past but, like many atomic physics activities, has not been pursued actively in recent years. The work probably had its start with the measurement of the absorption coefficient for slow electrons in gases by Lenard [4] and later by Ramsauer [5] and Mayer [6]. The method used by Ramsauer and several succeeding workers made use of a series of slits arranged in a circle with the electron paths being bent into this circle by a magnetic field. A measure of the emission current of the filament (electron beam source) and the current collected at the end of the path yielded the total

---

\* Numbers in brackets refer to entries in the Bibliography.

attenuation and hence a total collision probability. Data were obtained for a number of elements, and relatively good agreement between individual workers may be found in the energy range of about 4 to 100 ev. Total collision cross sections with electrons are available for such things as  $H_2$ , He, A, Ne,  $N_2$ , CO,  $CO_2$ , Xe, and Kr. However, note that only molecular cross sections are available for diatomic elements. Further, a rather general state of experimental disagreement exists at lower energies, which are of interest from the standpoint of plasma physics. Figure 1, taken from Brown's book [7] on plasma physics, is an example of data at this lower energy range. Practically no data for other elements is available. This program therefore has as its purpose the determination of atom-electron collision cross sections using the new arc technique for the energy range of Figure 1 and for a selection of elements of present-day interest.

## 2.2 CROSS-SECTION DETERMINATIONS USING THE ELECTRIC ARC

Experimental work can be performed using a stable, cylindrically symmetric arc operating at approximately 1 atmosphere of pressure. The element of interest can in principle be introduced either as the ambient gas or by a controlled process of electrode erosion.

Now the relation between electrical conductivity, the current density, and the electric field strength is given by Ohm's law as

$$\sigma = \frac{J}{E} \quad (1)$$

The electrical conductivity  $\sigma$  can be measured directly, and it is also possible to obtain the temperature distribution in an arc by spectroscopic

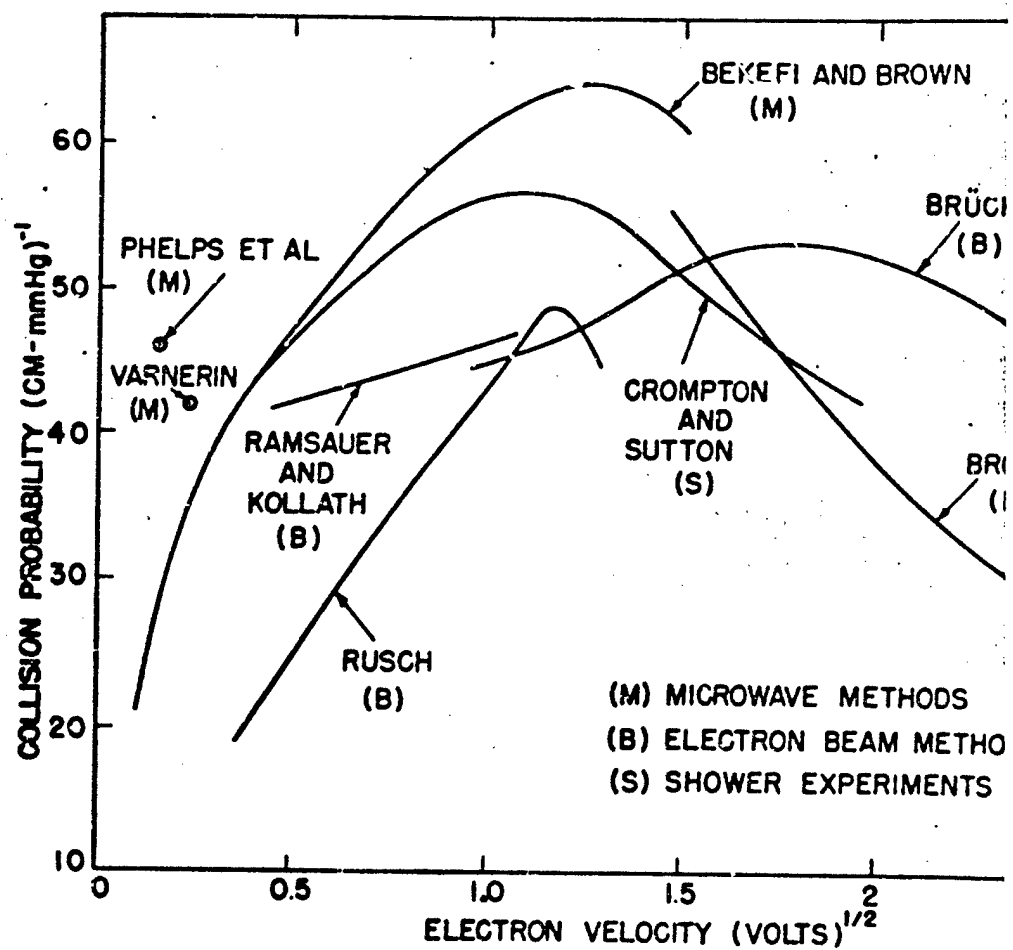
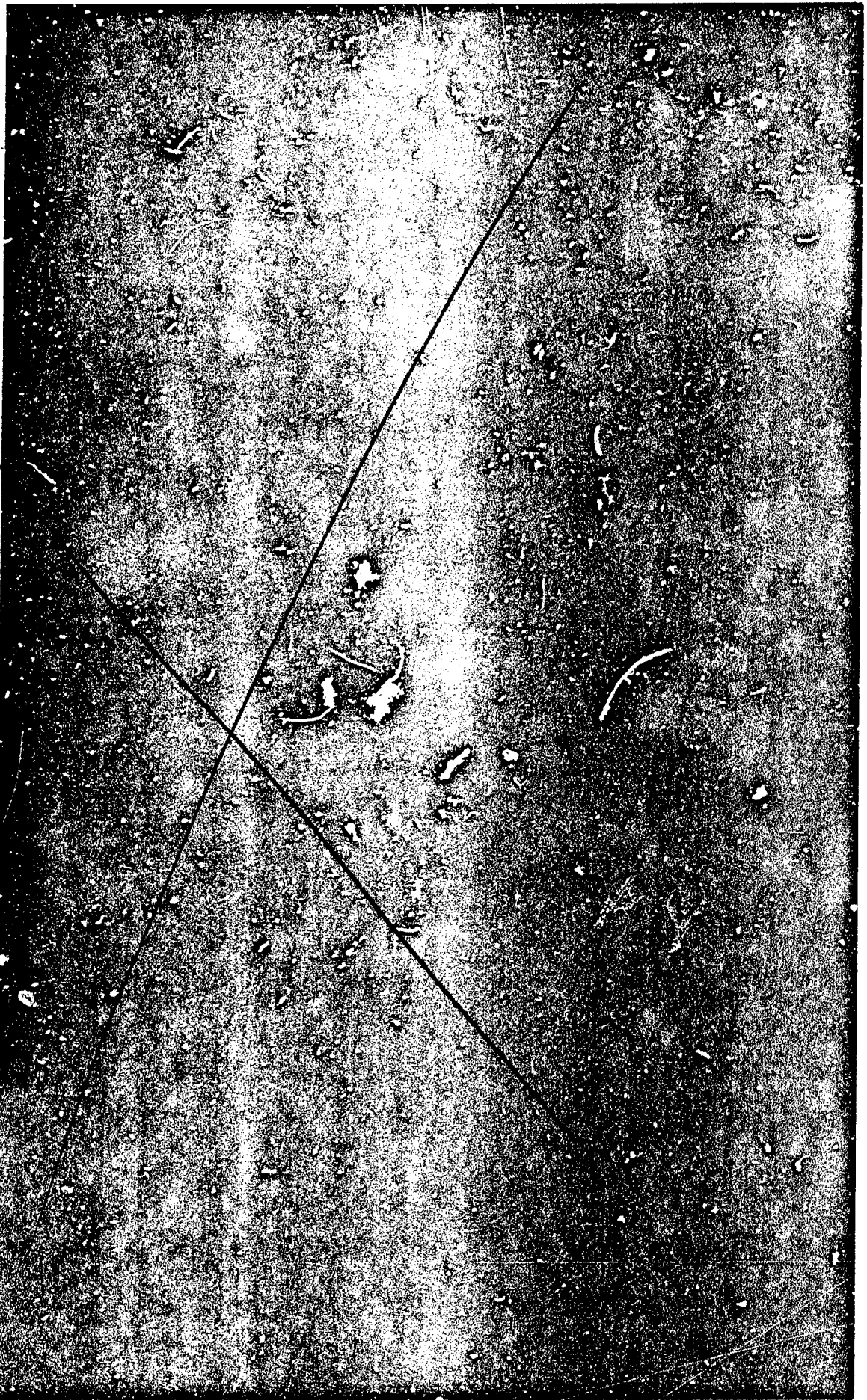


Figure 1. Low-Energy Collision Probabilities in Hydrogen



techniques. Therefore, a relation between temperature and conductivity must be obtained using the concept of charge transport by electrons in the arc plasma. In obtaining this relation, one can neglect the contribution of the ions because of their much lower mobility.

In the simplest case, if  $v_e$  is the mean thermal velocity of electrons,  $\lambda_e$  the mean free path, and  $\tau_e$  the mean interval between collisions,

$$\tau_e = \frac{\lambda_e}{v_e} . \quad (2)$$

If the electron is in the presence of an electric field, then during the time  $\tau_e$  the electron falls freely in the electric field a distance

$$D = \frac{eE}{2m_e} \tau_e^2 , \quad (3)$$

where  $e$  is the electronic charge and  $m_e$  the mass of the electron. Thus the average velocity (drift velocity) in the direction of the electric field is

$$u_e = \frac{D}{\tau_e} = \frac{e\lambda_e}{2m_e v_e} E . \quad (4)$$

This gives the electron mobility, in terms of the mean free path and thermal velocity, as

$$b_e = \frac{e\lambda_e}{m_e v_e} . \quad (5)$$

It should be realized that in the general case the mobility is a function of the electric field strength. However, a simple calculation shows that for the conditions of the experiment, Eq. (5) is a good approximation. As long as the electron temperature  $T_e$  is approximately equal to the heavy particle temperature (gas temperature)  $T_M$ , the drift is proportional to the electric field as given above. Now the electronic temperature becomes considerably different from the gas temperature when  $\lambda_e E$  increases beyond the value given by

$$\lambda_e E = \frac{1}{\epsilon} \sqrt{\frac{m_e}{M}} T_M, \quad (6)$$

where  $\epsilon$  is the conversion factor between electron volts and temperature. The R. H. S. of Eq. (6) is  $\geq 0.03$  for the energy range of interest. Further,  $\lambda_e$  can be taken as approximately  $10^{-3}$  cm for the condition at which our arc operates (atmospheric pressure and greater than  $10^4$  °K). Thus the electric field should generally be  $\leq 30$  volts/cm for our approximation to be valid and for complete equilibrium to be maintained. All data presented in this report correspond to field strengths well below this critical value.

Once again now, using Ohm's law, one finds that the electrical conductivity can be expressed as

$$\sigma = \frac{e^2 n_e \lambda_e}{m_e v_e}. \quad (7)$$

If one now introduces the gas-kinetic relation for the thermal velocity and expresses the mean free path in terms of the collision cross sections  $Q$ , the conductivity is related to the temperature, electron and atom

concentrations, and cross sections of atoms and ions against electrons by the expression

$$\sigma = \frac{J}{E} = \frac{e^2 n_e}{\left(\frac{8mKT}{\pi}\right)^{1/2}} \cdot \frac{1}{n_a Q_e^a + n_i Q_e^i} \quad (8)$$

In general, the symbol  $Q_j^k$  is used in this report to denote the total effective collision cross section for particles of kind  $j$  against particles of kind  $k$ . Note that if necessary the term  $n_a Q_e^a$  can be divided in the presence of several atom species into  $n_1 Q_1 + n_2 Q_2 + \dots$  and the term  $n_i Q_e^i$  into  $n_+ Q_+ + n_{++} Q_{++} + \dots$  in the presence of ions of multiple charge.

At this point it becomes necessary to discuss the geometry of the particular arc used in the experiments. Figure 2 shows this arc chamber along with electrode shapes and cooling water flow channels. Normally all parameters associated with an arc are functions of the column radius, so that spatially resolved measurements are required. However, Olsen [8] has shown that for the geometry used here the electric field is not a function of radius in the vicinity of the flat anode. Thus a single measurement of the field strength determines its value for all arc radii in this region. The current density, on the other hand, is a strong function of radius. The same is true for the temperature and number densities, which are related by the Saha equation and are measured spectroscopically. Measurements of these latter parameters then along with the field strength, in conjunction with the use of Eq. (8), provide the means for determining the cross sections as functions of the arc radius or plasma temperature. The temperature range that one can conveniently cover by this method lies approximately between 1 and 2 ev, with extensions possible under certain conditions.



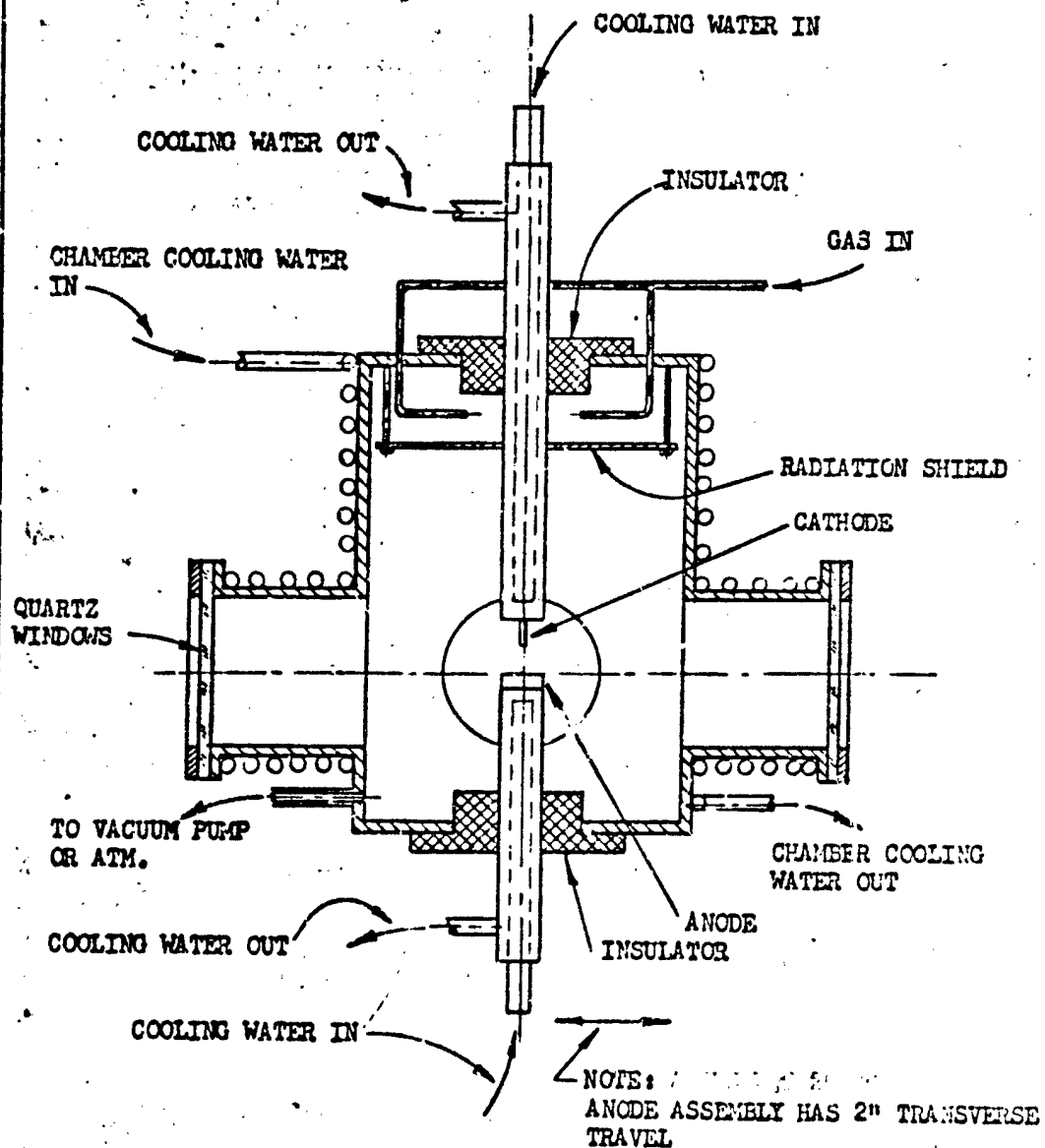


FIG. 2 SCHEMATIC DIAGRAM OF THE EXPERIMENTAL ARC CHAMBER

### 2.3 EXPERIMENTAL PREPARATIONS

At the outset of the program, this laboratory had had considerable experience in the development and operation of various arc plasma generators working at atmospheric pressure and with "vacuum arcs" operating at low pressures ( $\approx 10^{-6}$  mm Hg) and in strong magnetic fields. It was originally planned to modify one of these arcs for use in making the cross-section measurements. However, work on these arcs immediately prior to starting this program showed extreme turbulence and instabilities in the case of the atmospheric pressure arcs and a lack of thermodynamic equilibrium for the vacuum arcs. It was necessary, therefore, as a first step in this research, to design and construct an arc which could operate at about one atmosphere of pressure, be free of any major instabilities, and also be free of contamination due to electrode erosion. The design finally chosen as being most favorable is similar to one used by Olsen [8] in making transition probability measurements. It is relative simple (see Figure 2) and had been shown to be extremely stable in operating characteristics.

The electrical power for the arc is provided by a set of three motor-generator sets, with several series or parallel combinations available. A maximum of 365 volts is available at 200 amps, or a maximum current of 900 amps can be obtained at 120 volts. A ballast resistor, constructed in our shop, is used in series with the arc to provide the customary "drooping" volt-ampere characteristics for the power supply.

When first put into use, it was necessary to qualitatively assess the arc operation and to investigate briefly such parameters as electrical power, cathode size, arc length, and gas flow rates and their effects on arc stability.

Experiments quickly showed the importance of cathode size. In order to cover a range of currents from, say, 50 amps to 400 amps, it is necessary to use cathode sizes ranging from 0.060 inch to 0.120 inch in diameter. It was found that at the lower currents the cathodes larger than that necessary to supply the needed emission led to arc wandering and general instability, and, of course, at the higher currents the smaller cathodes suffered from erosion. Thus it is not possible to use any one cathode to cover the entire current range of interest.

The cathode material used has been 2 per cent thoriated tungsten in all cases. The anode material has been either copper, molybdenum, or tungsten, depending on the type of gas used for the experiment. During the first half of the program, it became clear that within the scope of this first year's effort probably three gases could be investigated. The three that were chosen, and for which the necessary computations were started, were argon, helium, and nitrogen. All these gases used for the experiment were certified to have less than 10 ppm of any impurity and were at least 99.997 per cent pure over-all. Argon and helium worked well with any anode, as may well have been expected. However, it was found to be impossible to operate a pure nitrogen arc without considerable erosion of any anode surface. Since erosion leads to contamination of the arc plasma by atoms of the electrode, this condition could hardly be tolerated. A solution was found by using a mixture of argon and nitrogen. As long as argon is present at 50 per cent partial pressure or greater, the copper anode can be used with negligible erosion. Continuous four-hour operation with no change in arc parameters indicates that a steady plasma free of contamination is obtained.

The precise ratio of gases to be used in this case was measured in the following way: Using the settings of regulator valves on argon and nitrogen gas cylinders which correspond to desired arc operation, the flow rates of argon and nitrogen were independently measured. A manometer was used to insure that individual pressures did not exceed atmospheric pressure by more than  $1/2$  cm Hg and did not differ from each other by more than  $1/4$  cm Hg.

When the gases passed from the high-pressure cylinder into the line leading to the chamber, they were cooled because of expansion. A large length of this line was used to warm the gas. The difference in temperature between the two gases was measured at the entrance of the flowmeter with a thermocouple. Knowing the pressure, temperature, and atomic weights of the two gases, their true flow rates were determined. This yielded the ratio, by volume, of argon to nitrogen. Since this ratio is kept constant during a running of the arc, a simple application of Dalton's law yields the particle number densities for each gas.

All experimental indications are that this arc besides being free of electrode contamination, is extremely stable in operation. High-speed motion pictures (4000 frames/sec) have indicated neither any visible fluctuations in arc intensity with time nor any spatial inhomogeneity. Photoelectric measurements of the total intensity of the arc have not revealed any fluctuations up to frequencies of 10 megacycles/sec, the limit of the measurements. Oscilloscope traces of arc voltage show a fluctuation of less than 1 per cent at a kilocycle and a megacycle, with all other perturbations being negligible. Thus it appears that the arc,

operating at atmospheric pressure, provides a steady-state, uncontaminated plasma with local thermodynamic equilibrium well established. Typical operation, shown for the case of argon at 50 amps and an arc length of  $1/2$  inch, is seen in Figure 3. Figure 4 is a photograph of the arc chamber and associated equipment, showing the 3.4-meter Ebert spectrograph in the background. Figure 5 shows the flat voltage-current characteristic for the gases and power ranges used for the experiments. The voltage rises sharply, of course, when the current approaches zero for all three cases.

## 2.4 PRELIMINARY CALCULATIONS

A number of computations were necessary so that experimental results could be used to deduce values for collision cross sections. In all cases, the work was done using a desk calculator. Although the establishment of a numerical program may have been justified for obtaining number densities, partition functions, etc., it was felt this procedure would not prove economical within the scope of the program.

For all of this work and for the spectroscopy that follows, we assume that LTE prevails, that is, that the kinetic temperatures of electrons, atoms, and ions and also the temperatures characterizing the distributions over bound states (Boltzmann factors) and free states (Saha equations) are alike. This assumption is justified by the facts that, for our range of temperatures and pressures, excitation and de-excitation by electron collisions are predominant and that our voltages in the arc column are less than the critical potentials (see Eq. 6 and Figure 5).

The partition functions and number densities for argon were taken directly from values tabulated by Olsen [8]. The particle densities

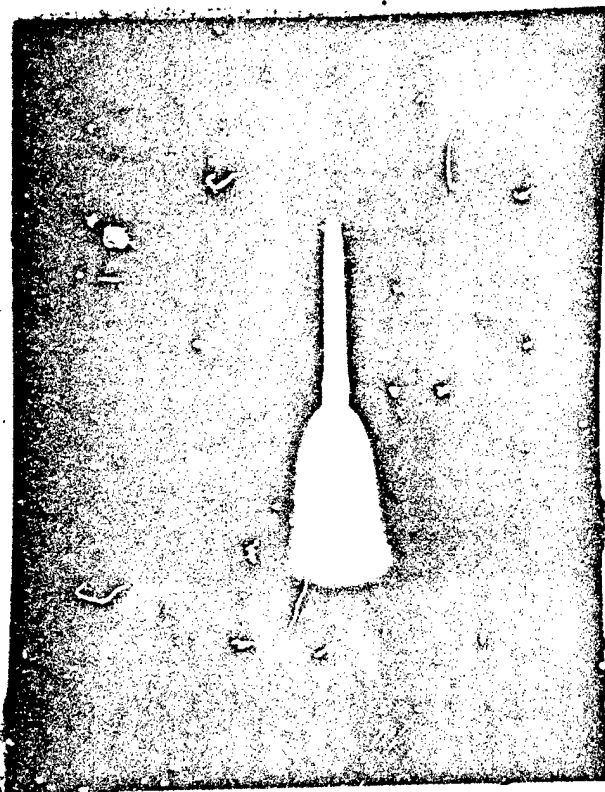


FIG. 3      PHOTOGRAPH OF ARC OPERATING AT 50 AMPS  
IN ARGON AT A LENGTH OF  $1/2$  INCH.

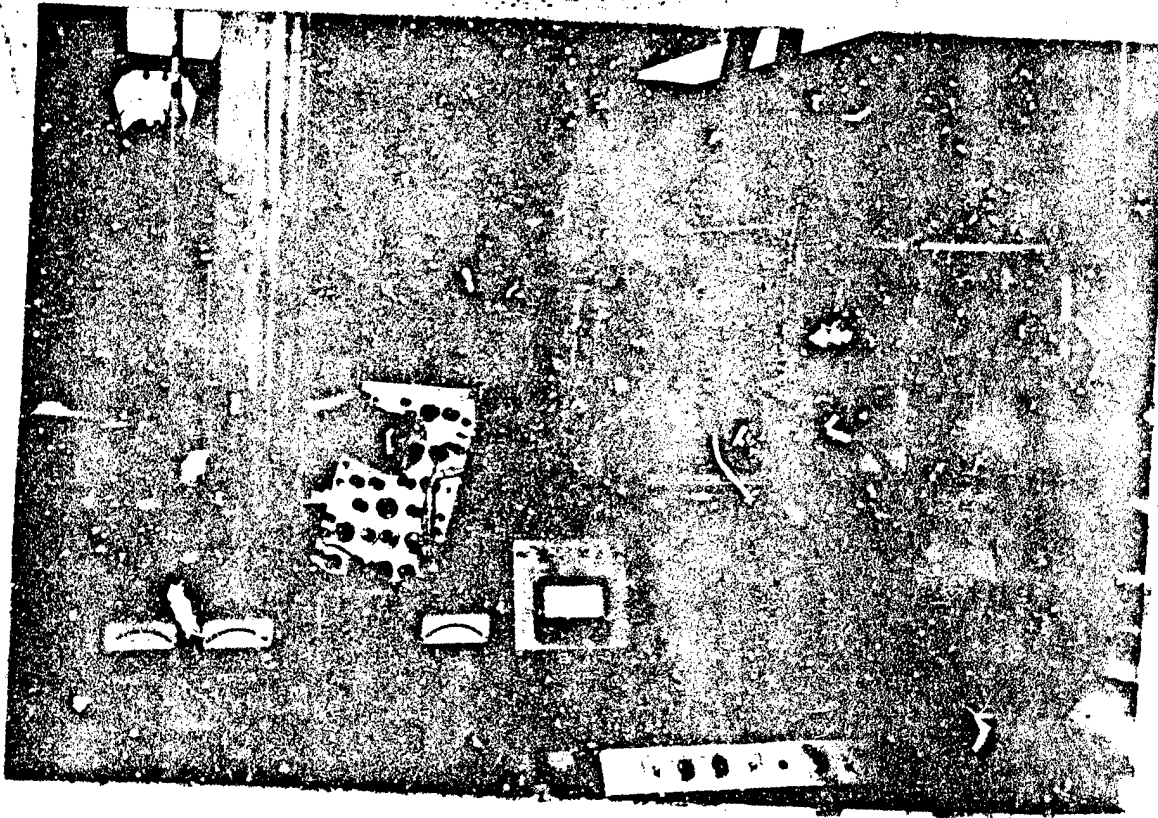
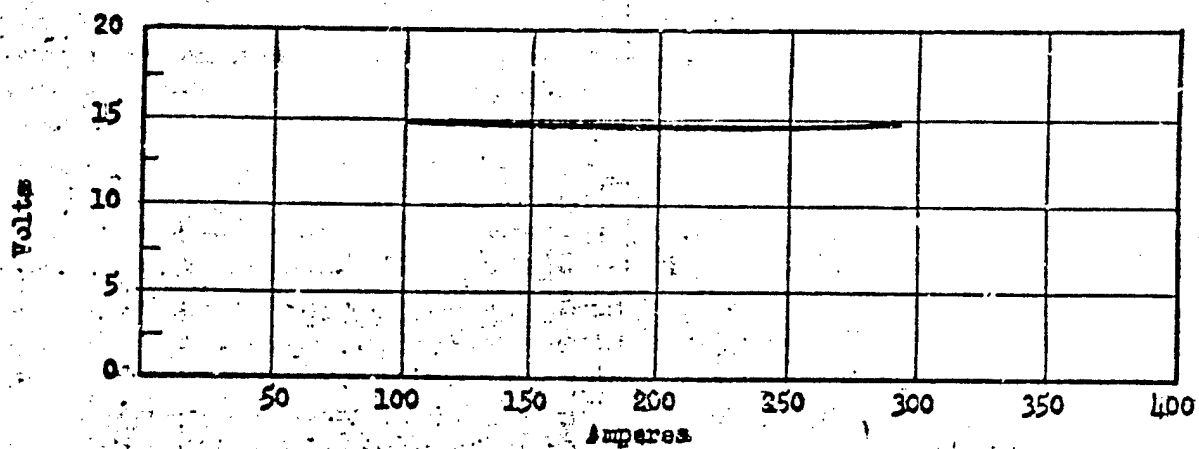
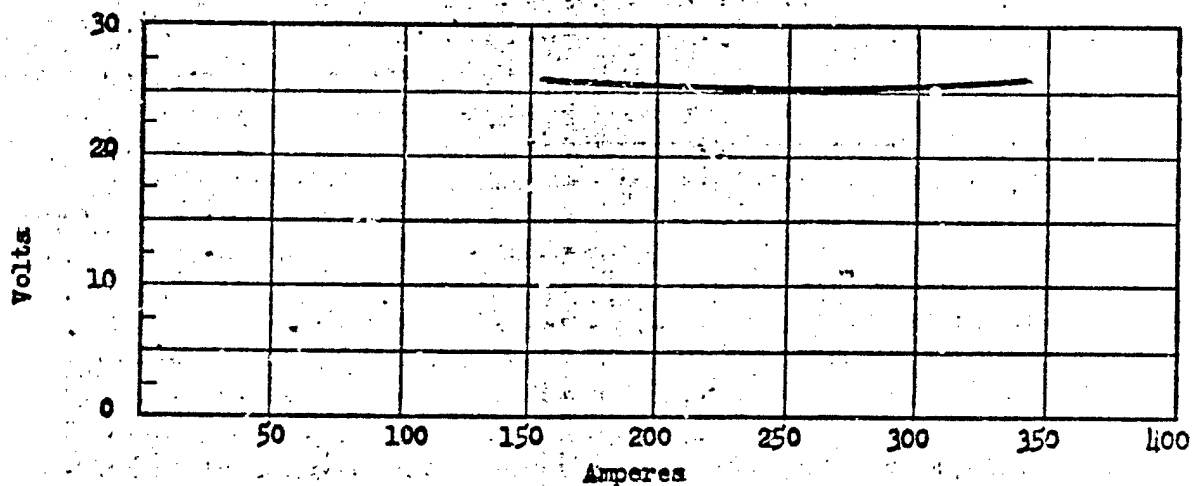


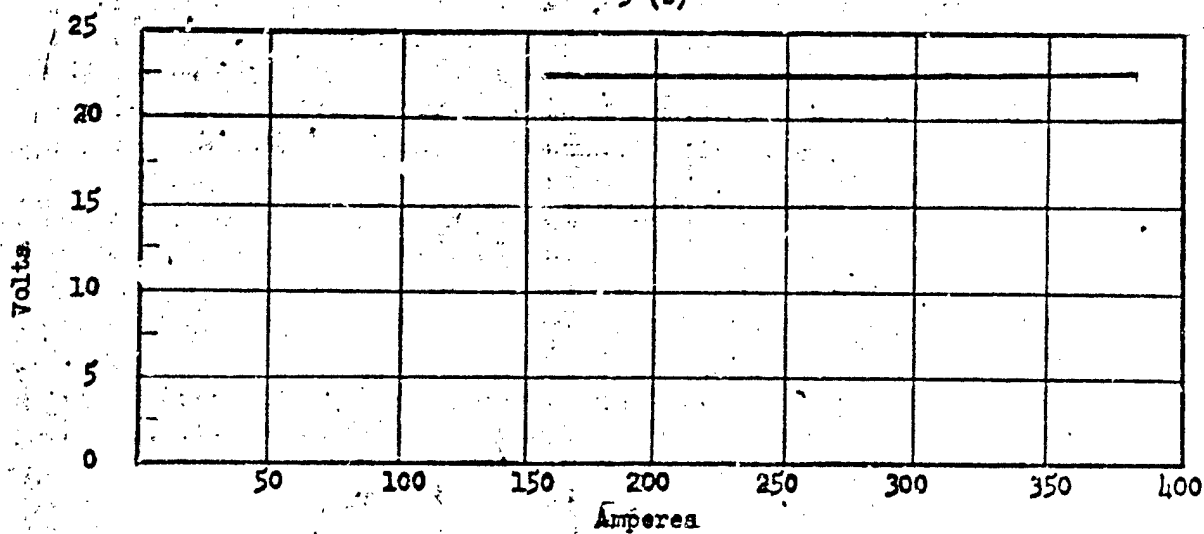
FIG. 4 PHOTOGRAPH OF ARC CHAMBER AND ASSOCIATED EQUIPMENT



5 (a)



5 (b)



5 (c)

FIG. 5 VOLTAGE-CURRENT CHARACTERISTICS FOR 3/8" ARC USING: a) ARGON; b) HELIUM; AND c) 66% ARGON, 34% NITROGEN.



for the temperature range of interest are given in Figure 6, where  $n_0$  is the number density of atoms,  $n_+$  of singly charged ions,  $n_e$  of electrons, and  $N$  the total particle density. In all cases the presence of doubly charged ions were tabulated. However, since their density is relatively small at these temperatures, they were omitted from the figures for the sake of convenience. The partition functions for helium were obtained from data presented by Barr, Cason, and Smith [9, 10]. Using this information, one can solve a set of equations (Saha relation, charge neutrality, Dalton's law) and obtain the particle densities in helium as a function of temperature. These data are given in Figure 7 for the case of atmospheric pressure.

The number densities for a pure nitrogen gas at atmospheric pressure had been tabulated by Burhorn and Wienecke [11] (see Figure 8), and it was at first anticipated that these data could be applied directly to a nitrogen arc. However, subsequent arc operation showed that severe electrode erosion always occurred in a pure nitrogen atmosphere. Data was therefore needed for a mixture of 34 per cent nitrogen, 66 per cent argon, which proved to operate satisfactorily. This was obtained by using the partition functions for nitrogen calculated by Cason and Smith [10], the partition functions for argon mentioned above, and solving a set of equations which were similar to, though more complicated than, those for the case of helium mentioned above.

The next step in the series of calculations is to make use of these number densities in calculating the ion-electron collision cross sections. At the outset of this program, it was not certain whether theoretical or experimental values should be obtained for these cross sections (these values are needed for the final calculations when obtaining atom-electron cross sections). A literature survey along with an estimate of these further experimental costs strongly favored the analytical method.

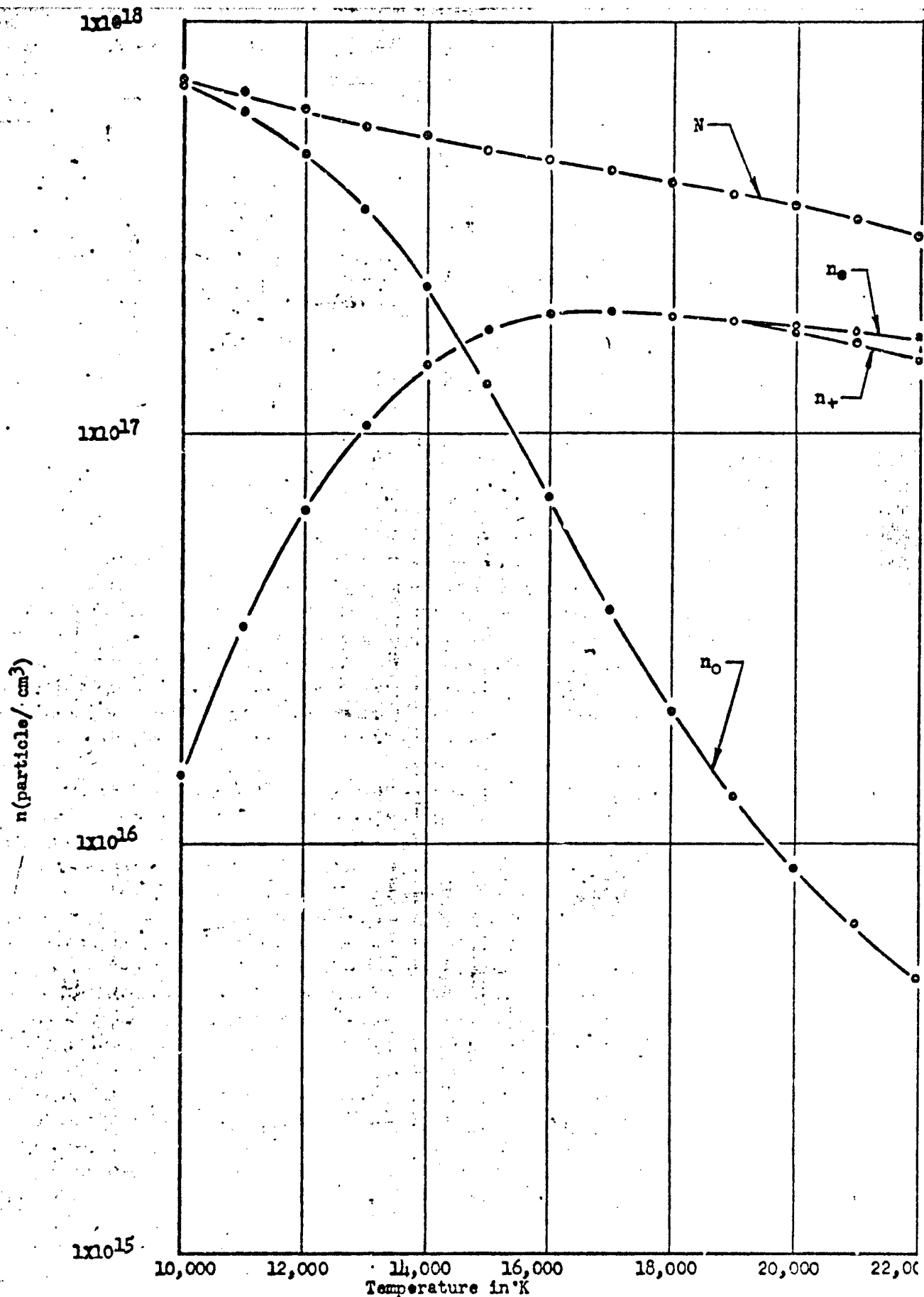


FIG. 6 PARTICLE DENSITIES FOR AN ATMOSPHERIC PRESSURE ARGON PLASMA

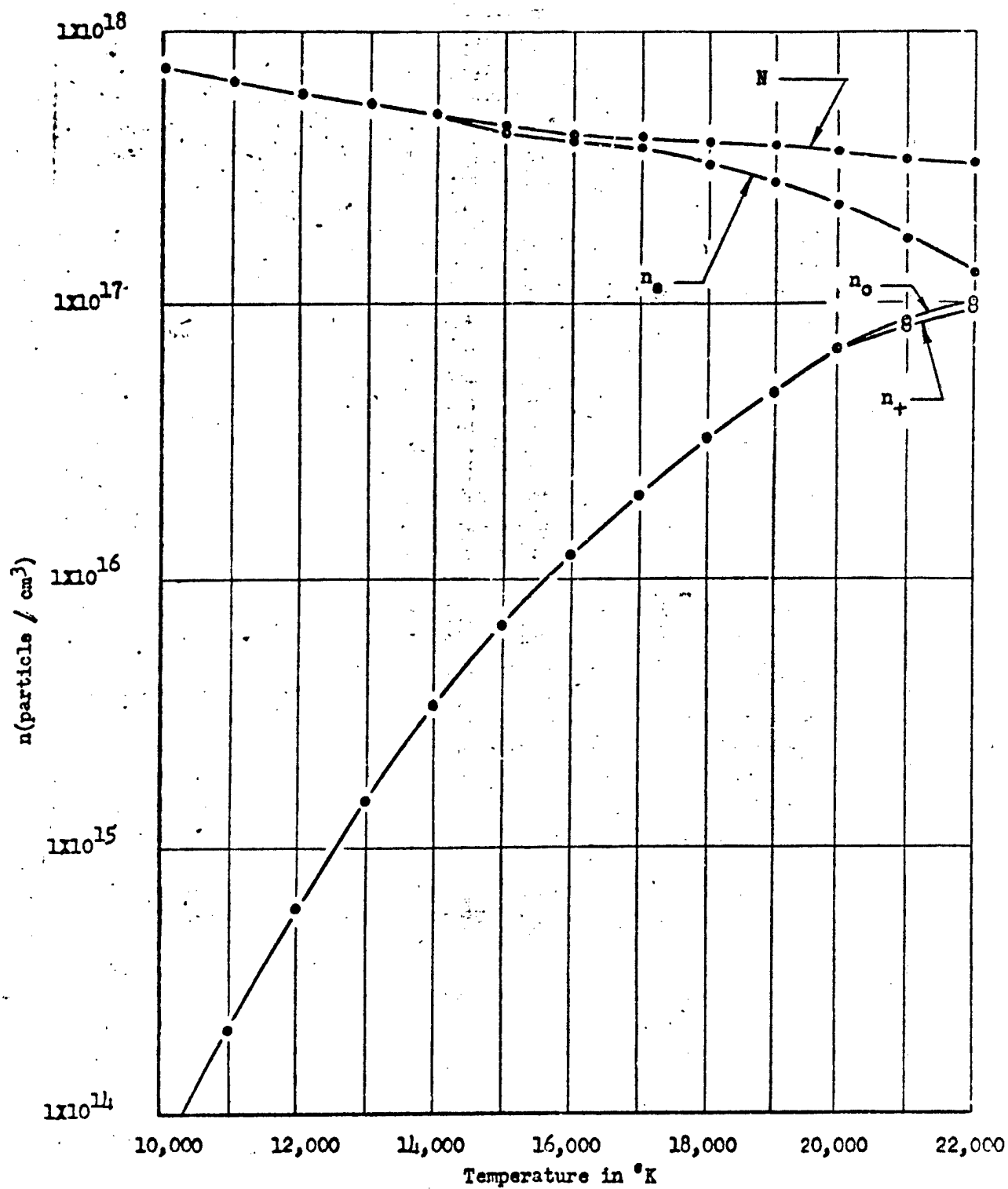


FIG. 7 PARTICLE DENSITIES FOR AN ATMOSPHERIC PRESSURE HELIUM PLASMA

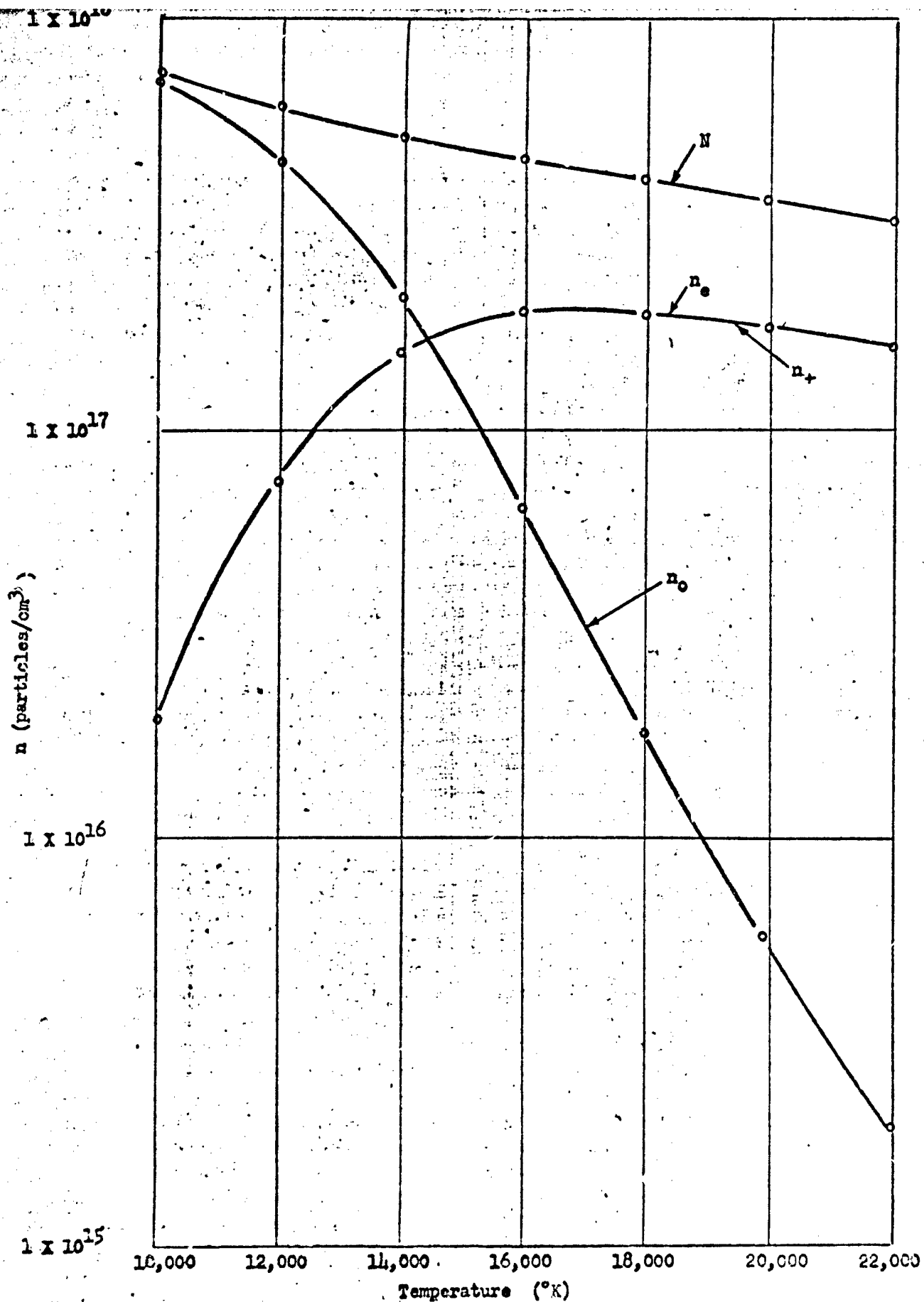


FIG. 8 PARTICLE DENSITIES FOR AN ATMOSPHERIC PRESSURE NITROGEN PLASMA

Now in order to obtain a relation for the ion-electron cross section, we can make use of Eq. (7) and rewrite it in the form

$$\sigma = \frac{e^2 n_e \lambda_e}{(3 m K T)^{1/2}} \quad (9)$$

According to Spitzer and Härm [12, 13], the electrical conductivity of a completely ionized gas is given by

$$\sigma = \frac{2 (K T)^{3/2} \gamma_E}{\left[ \left( \frac{\pi}{2} \right)^{3/2} (m_e)^{1/2} e^2 Z \ln q \right]} \quad (10)$$

where

$$Z = \sum_i \frac{n_i Z_i^2}{n_e}, \quad q = \frac{K T}{e^2 Z n_+^{1/3}}$$

$n_+$  is the number of ions/cm<sup>3</sup> having an effective charge  $Z$  per ion, and  $\gamma_E$  is a coefficient tabulated by Spitzer. This expression can be equated to the gas-kinetic expression (Eq. 9) for the case where  $\lambda_e$  contains no dependence on atoms and the ion-electron cross sections ( $Q_e^i$ ) thereby obtained. This treatment by Spitzer apparently considers the mutual effect of electrons upon one another as contrasted with Gvosdovers theory, which will be mentioned below. The greatest uncertainty in Eq. (10) exists in the numerical value of the  $(\ln)$  term. Equating Eqs. (9) and (10) gives the following expression:

$$\sum_i n_i Q_e^i = \left[ \frac{\left( \frac{\pi}{2} \right)^{3/2} \left( \frac{1}{3} \right)^{1/2}}{2} \right] \frac{e^4 n_e Z \ln q}{(K T)^2 \gamma_E} \quad (11)$$

Since we are interested in the temperature range below some 20,000°K, a simplification can be made. That is, that singly charged ions are the predominant ion species present. The R. H. S. of Eq. (11) is then simply  $n_i Q_i^e$ . Further, cancelling the  $n_i$  and  $n_e$ , the expression finally becomes

$$Q_i^e \approx (.4) \frac{\pi}{2} \frac{e^4}{(KT)^2} Z \frac{\ln g}{\gamma_E} \quad (12)$$

This is about half the value obtained by Gvosdover and Peters [14, 15] and is in good agreement with the preliminary results obtained in [18]. For  $Z = 1$  and  $\gamma_E = 0.5816$ , one obtains within the accuracy of the measurements ( $\approx \pm 10\%$ ) the simple expression

$$Q_i^e = \frac{e^4}{(KT)^2} \ln \left( \frac{KT}{e^2 n_i^{1/3}} \right) \quad (13)$$

Using the Rutherford scattering formula as applied to ions with charge  $Z$ , this can be converted to

$$Q_{Z+} = Z^2 Q_+ \quad (14)$$

Calculations based on these relations were made for the three gases, argon, helium, and nitrogen, for the appropriate temperature ranges. The results are shown in Figures 9, 10, and 11. Experimentally, of course, nitrogen was mixed with argon in a known ratio so as to prevent erosion. Therefore, in all calculations for this argon-nitrogen mixture, the nitrogen cross section data were combined with that for argon so that the terms  $n_a Q_e^a$  and  $n_i Q_e^i$  in Eq. (8) were actually sums over all the species present at their relative concentrations.

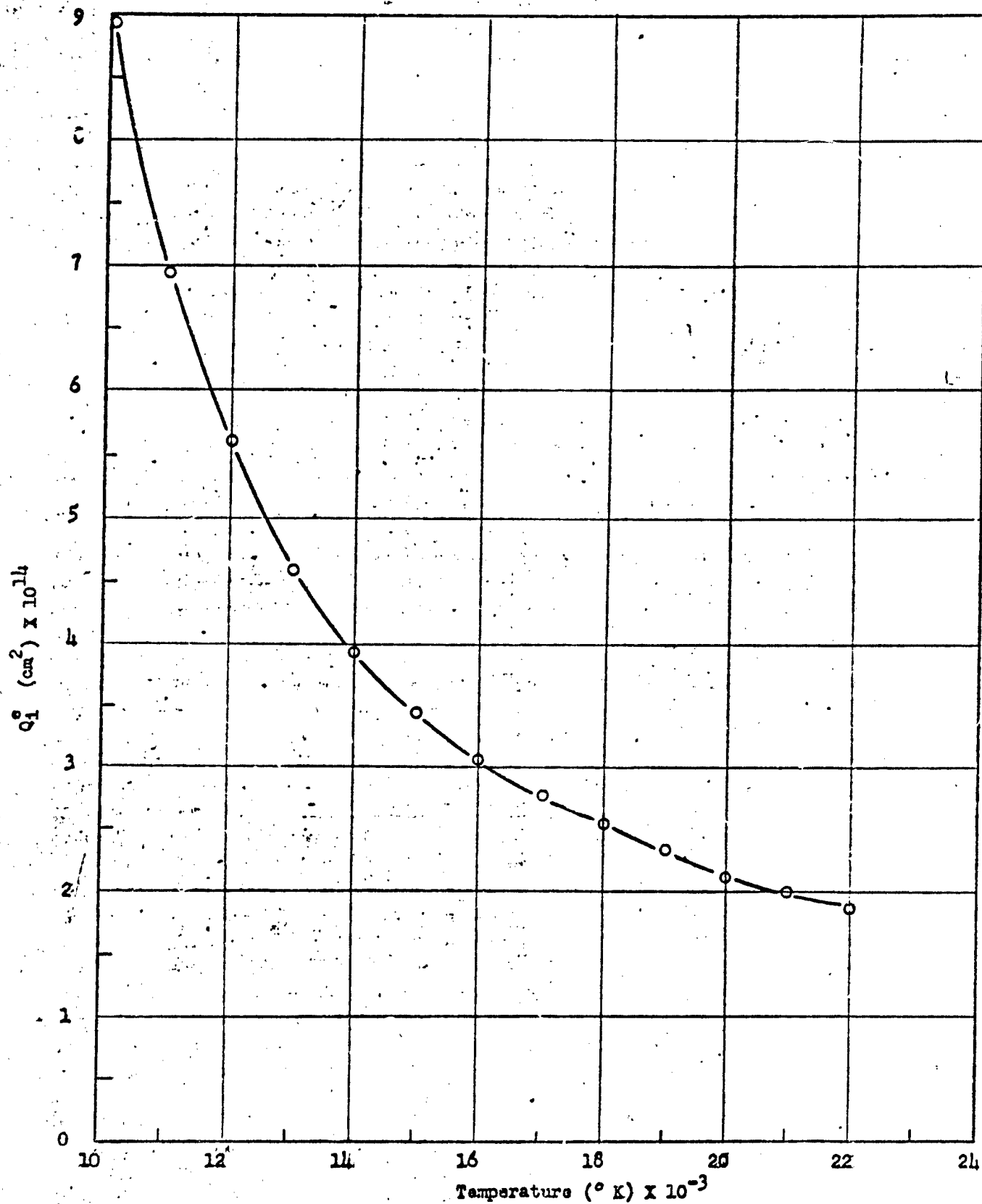


FIG. 9 ION-ELECTRON CROSS-SECTIONS FOR ARGON AT ATMOSPHERIC PRESSURE.

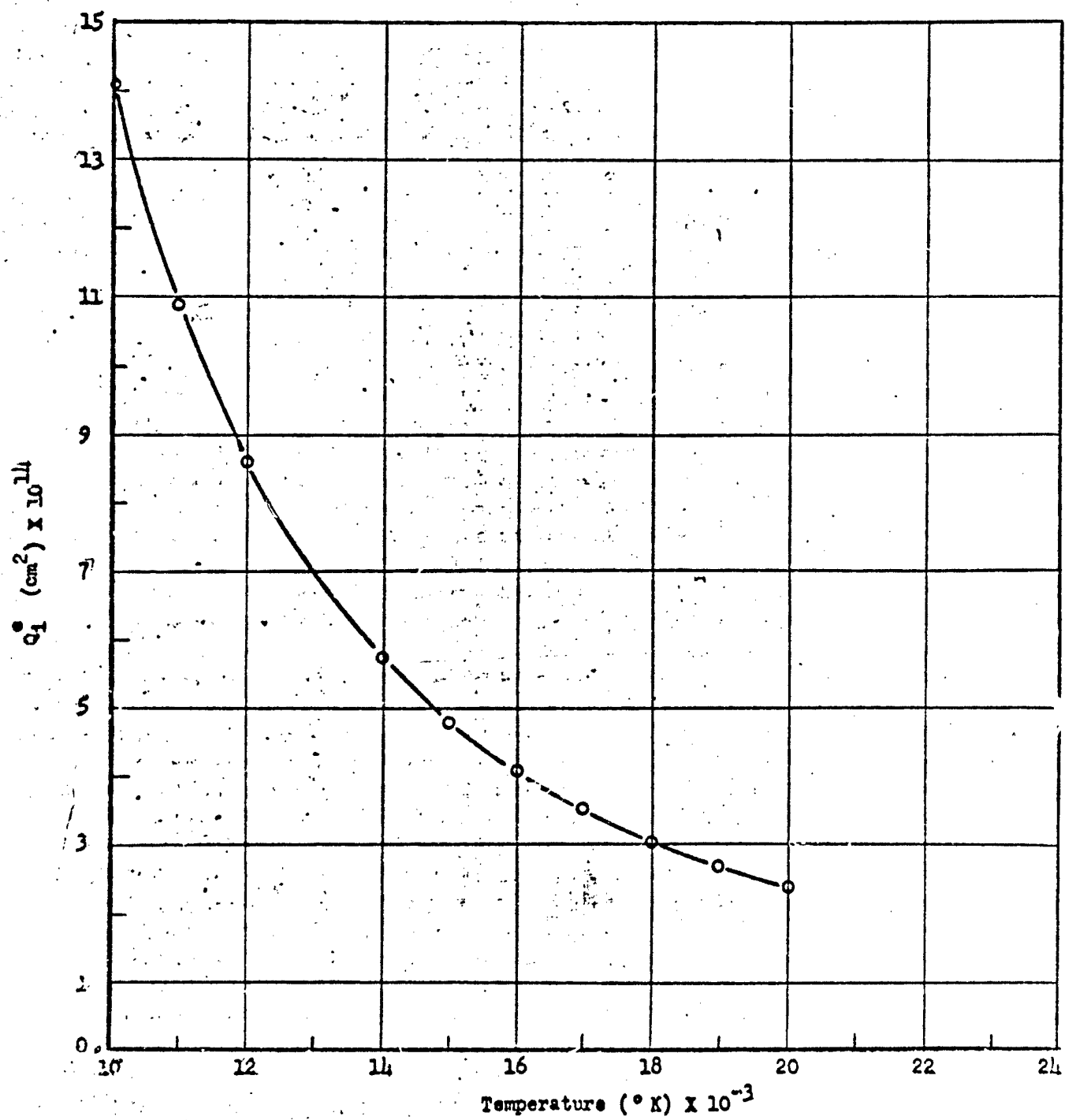


FIG. 10 ION-ELECTRON CROSS-SECTIONS FOR HELIUM AT ATMOSPHERIC PRESSURE.



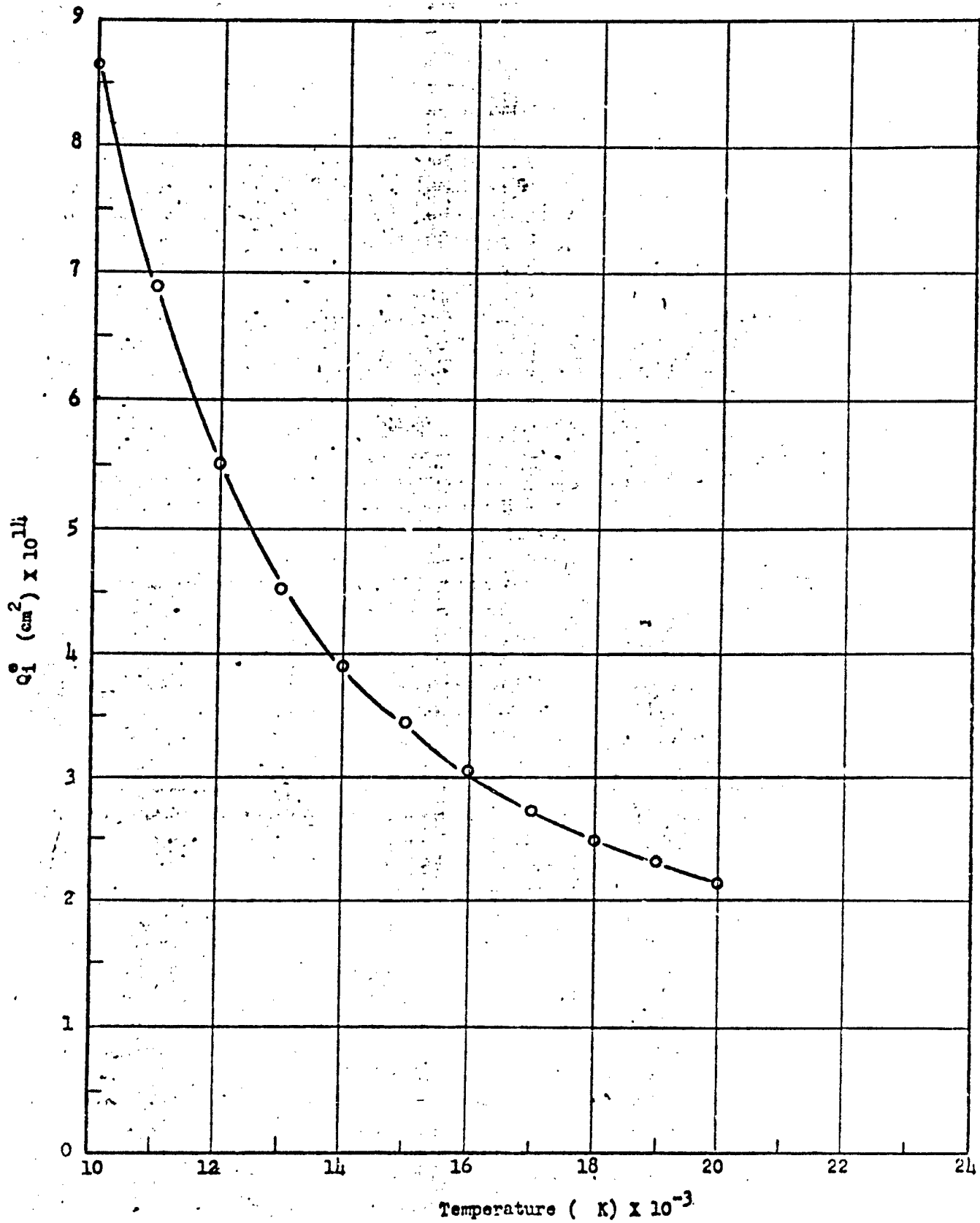


FIG. 11 ION-ELECTRON CROSS-SECTIONS FOR NITROGEN AT ATMOSPHERIC PRESSURE.

## 2.5 GENERAL COMMENTS ON SPECTROSCOPIC TEMPERATURE MEASUREMENTS

In recent years, with the advent of plasma physics studies in the laboratory, several new methods for making spectrometric measurements of high temperatures have been added to those which already had been developed by the astrophysicists. A review [16] of these methods shows the wide variety of techniques which are applied to different types of plasmas at different energy or temperature levels.

For our case, with a plasma at one atmosphere of pressure and at temperatures less than  $25,000^{\circ}\text{K}$ , the most likely methods involve the calculation of temperatures from measurements of intensity ratios of emitted spectral lines, from measurements of spectral line broadening caused by the emitting atom's collisions with other particles, or by making use of the radial intensity inversion of spectral lines emitted by cylindrical sources under certain conditions. Where necessary, these techniques will be described in some detail below. It is sufficient to say here that the choice of any one of these methods is determined largely by the ionization potential and type of spectra emitted by a particular element of interest. Any of these methods, of course, requires certain knowledge of spectroscopic quantities, such as energy levels, transition probabilities, line broadening coefficients, etc. In general, much of this information is lacking. However, recent work has been done for argon, nitrogen, and helium. In particular, the latest values for argon transition probabilities were obtained from H. N. Olsen [17], data on helium were obtained from W. B. Johnson [18] and A. T. Hattenberg [19], and nitrogen transition probabilities from data published by J. Richter [20].

Now in order to apply any of these techniques to measuring the temperature of an arc, it should be realized that a correction must be made when observing the intensity of radiation emitted from an optically thin cylindrical source. When observed from the side, the volume of such a source under observation is in the shape of a disk viewed edge-on. That is, an observer some distance from the side of this disk, when looking at a point on the arc surface, receives radiation emitted by many regions in the arc's interior behind this point. Since the depth of these regions is a function of arc radius, a relation must be used to transform the observed transverse intensity to a true radial intensity. Such a relation is the Abel integral equation,

$$I(x) = 2 \int_{r=x}^R \frac{I(r) r dr}{r^2 - x^2} , \quad (15)$$

where  $I(x)$  is the observed transverse intensity and  $I(r)$  is the true radial intensity. This procedure has been described in detail elsewhere [21], but for the sake of completeness, mention is made here of the fact that we had in the past used a numerical technique in obtaining  $I(r)$  as a function of  $I(x)$  from the relation

$$I(r_i) = \sum_{j=1}^n \alpha_{ij} I(x_j) . \quad (16)$$

The coefficients in this relation, which are used in this present program for all the spectroscopic work, are given in Table 1.

Table 1. Values of  $\alpha_{ij}$  Used to Transform Observed Into

	1	2	3	4	5	6	7	8	9	10	11	12	13	14	15
1	0.00000	0.00000	0.00000	0.00000	0.00000	0.00000	0.00000	0.00000	0.00000	0.00000	0.00000	0.00000	0.00000	0.00000	0.00000
2	0.00000	0.00000	0.00000	0.00000	0.00000	0.00000	0.00000	0.00000	0.00000	0.00000	0.00000	0.00000	0.00000	0.00000	0.00000
3	0.00000	0.00000	0.00000	0.00000	0.00000	0.00000	0.00000	0.00000	0.00000	0.00000	0.00000	0.00000	0.00000	0.00000	0.00000
4	0.00000	0.00000	0.00000	0.00000	0.00000	0.00000	0.00000	0.00000	0.00000	0.00000	0.00000	0.00000	0.00000	0.00000	0.00000
5	0.00000	0.00000	0.00000	0.00000	0.00000	0.00000	0.00000	0.00000	0.00000	0.00000	0.00000	0.00000	0.00000	0.00000	0.00000
6	0.00000	0.00000	0.00000	0.00000	0.00000	0.00000	0.00000	0.00000	0.00000	0.00000	0.00000	0.00000	0.00000	0.00000	0.00000
7	0.00000	0.00000	0.00000	0.00000	0.00000	0.00000	0.00000	0.00000	0.00000	0.00000	0.00000	0.00000	0.00000	0.00000	0.00000
8	0.00000	0.00000	0.00000	0.00000	0.00000	0.00000	0.00000	0.00000	0.00000	0.00000	0.00000	0.00000	0.00000	0.00000	0.00000
9	0.00000	0.00000	0.00000	0.00000	0.00000	0.00000	0.00000	0.00000	0.00000	0.00000	0.00000	0.00000	0.00000	0.00000	0.00000
10	0.00000	0.00000	0.00000	0.00000	0.00000	0.00000	0.00000	0.00000	0.00000	0.00000	0.00000	0.00000	0.00000	0.00000	0.00000
11	0.00000	0.00000	0.00000	0.00000	0.00000	0.00000	0.00000	0.00000	0.00000	0.00000	0.00000	0.00000	0.00000	0.00000	0.00000
12	0.00000	0.00000	0.00000	0.00000	0.00000	0.00000	0.00000	0.00000	0.00000	0.00000	0.00000	0.00000	0.00000	0.00000	0.00000
13	0.00000	0.00000	0.00000	0.00000	0.00000	0.00000	0.00000	0.00000	0.00000	0.00000	0.00000	0.00000	0.00000	0.00000	0.00000
14	0.00000	0.00000	0.00000	0.00000	0.00000	0.00000	0.00000	0.00000	0.00000	0.00000	0.00000	0.00000	0.00000	0.00000	0.00000
15	0.00000	0.00000	0.00000	0.00000	0.00000	0.00000	0.00000	0.00000	0.00000	0.00000	0.00000	0.00000	0.00000	0.00000	0.00000

### Radial Intensities\*

16	17	20	21	22	23	24	25
+ 301138	- 300931	300837	300737	300639	300542	300478	300351
- 301150	300938	300843	300743	300645	300547	300483	300352
- 301171	300955	300857	300754	300653	300546	300482	300358
- 3	300981	300878	300771	300671	300553	300484	300364
- 30120	300918	300808	300691	300578	300468	300386	300368
- 301112	300977	300866	300746	300621	300499	300377	300372
- 301256	301130	300988	300887	300754	300618	300468	300381
- 301400	301217	301063	300938	300838	300746	300678	300614
- 301546	301319	301147	301003	300887	300779	300711	300642
- 301703	301483	301348	301238	300952	300843	300753	300707
- 301846	301617	301468	301358	301036	300907	300804	300718
301938	301668	301543	301344	301134	300980	300867	300788
- 302116	301838	301691	301478	301287	301087	300948	300823
- 302276	301968	301868	301683	301417	301238	301044	300878
- 302473	302084	301911	301787	301513	301364	301191	301008
- 302672	302167	302068	301883	301723	301550	301378	301188
- 302877	302234	302167	301968	301788	301644	301483	301273
- 303066	302367	302301	302168	301946	301788	301611	301441
- 303268	302483	302403	302249	301973	301818	301678	301543
- 303468	302607	302544	302344	302126	301947	301788	301578
- 303668	302732	302668	302468	302240	302077	301818	301673
- 303868	302857	302793	302593	302364	302177	301918	301773
- 304068	302982	302918	302718	302488	302307	302048	301873
- 304268	303107	303043	302843	302613	302427	302168	301973
- 304468	303232	303168	302968	302738	302547	302288	302073
- 304668	303357	303293	303093	302863	302677	302418	302273
- 304868	303482	303418	303218	302988	302807	302548	302373
- 305068	303607	303543	303343	303113	302927	302668	302473
- 305268	303732	303668	303468	303238	303057	302798	302573
- 305468	303857	303793	303593	303363	303177	302918	302773
- 305668	303982	303918	303718	303488	303307	303048	302873
- 305868	304107	304043	303843	303613	303427	303168	302973
- 306068	304232	304168	303968	303738	303547	303288	303073
- 306268	304357	304293	304093	303863	303677	303418	303173
- 306468	304482	304418	304218	303988	303807	303548	303273
- 306668	304607	304543	304343	304113	303927	303668	303373
- 306868	304732	304668	304468	304238	304057	303798	303473
- 307068	304857	304793	304593	304363	304177	303918	303573
- 307268	304982	304918	304718	304488	304307	304048	303673
- 307468	305107	305043	304843	304613	304427	304168	303773
- 307668	305232	305168	304968	304738	304547	304288	303873
- 307868	305357	305293	305093	304863	304677	304418	303973
- 308068	305482	305418	305218	304988	304807	304548	304073
- 308268	305607	305543	305343	305113	304927	304668	304173
- 308468	305732	305668	305468	305238	305057	304798	304273
- 308668	305857	305793	305593	305363	305177	304918	304373
- 308868	305982	305918	305718	305488	305307	305048	304473
- 309068	306107	306043	305843	305613	305427	305168	304573
- 309268	306232	306168	305968	305738	305547	305288	304673
- 309468	306357	306293	306093	305863	305677	305418	304773
- 309668	306482	306418	306218	305988	305807	305548	304873
- 309868	306607	306543	306343	306113	305927	305668	304973
- 310068	306732	306668	306468	306238	306057	305798	305073
- 310268	306857	306793	306593	306363	306177	305918	305173
- 310468	306982	306918	306718	306488	306307	306048	305273
- 310668	307107	307043	306843	306613	306427	306168	305373
- 310868	307232	307168	306968	306738	306547	306288	305473
- 311068	307357	307293	307093	306863	306677	306418	305573
- 311268	307482	307418	307218	306988	306807	306548	305673
- 311468	307607	307543	307343	307113	306927	306668	305773
- 311668	307732	307668	307468	307238	307057	306798	305873
- 311868	307857	307793	307593	307363	307177	306918	305973
- 312068	307982	307918	307718	307488	307307	307048	306073
- 312268	308107	308043	307843	307613	307427	307168	306173
- 312468	308232	308168	307968	307738	307547	307288	306273
- 312668	308357	308293	308093	307863	307677	307418	306373
- 312868	308482	308418	308218	307988	307807	307548	306473
- 313068	308607	308543	308343	308113	307927	307668	306573
- 313268	308732	308668	308468	308238	308057	307798	306673
- 313468	308857	308793	308593	308363	308177	307918	306773
- 313668	308982	308918	308718	308488	308307	308048	306873
- 313868	309107	309043	308843	308613	308427	308168	306973
- 314068	309232	309168	308968	308738	308547	308288	307073
- 314268	309357	309293	309093	308863	308677	308418	307173
- 314468	309482	309418	309218	308988	308807	308548	307273
- 314668	309607	309543	309343	309113	308927	308668	307373
- 314868	309732	309668	309468	309238	309057	308798	307473
- 315068	309857	309793	309593	309363	309177	308918	307573
- 315268	309982	309918	309718	309488	309307	309048	307673
- 315468	310107	310043	309843	309613	309427	309168	307773
- 315668	310232	310168	309968	309738	309547	309288	307873
- 315868	310357	310293	310093	309863	309677	309418	307973
- 316068	310482	310418	310218	309988	309807	309548	308073
- 316268	310607	310543	310343	310113	309927	309668	308173
- 316468	310732	310668	310468	310238	310057	309798	308273
- 316668	310857	310793	310593	310363	310177	309918	308373
- 316868	310982	310918	310718	310488	310307	310048	308473
- 317068	311107	311043	310843	310613	310427	310168	308573
- 317268	311232	311168	310968	310738	310547	310288	308673
- 317468	311357	311293	311093	310863	310677	310418	308773
- 317668	311482	311418	311218	310988	310807	310548	308873
- 317868	311607	311543	311343	311113	310927	310668	308973
- 318068	311732	311668	311468	311238	311057	310798	309073
- 318268	311857	311793	311593	311363	311177	310918	309173
- 318468	311982	311918	311718	311488	311307	311048	309273
- 318668	312107	312043	311843	311613	311427	311168	309373
- 318868	312232	312168	311968	311738	311547	311288	309473
- 319068	312357	312293	312093	311863	311677	311418	309573
- 319268	312482	312418	312218	311988	311807	311548	309673
- 319468	312607	312543	312343	312113	311927	311668	309773
- 319668	312732	312668	312468	312238	312057	311798	309873
- 319868	312857	312793	312593	312363	312177	311918	309973
- 320068	312982	312918	312718	312488	312307	312048	310073
- 320268	313107	313043	312843	312613	312427	312168	310173
- 320468	313232	313168	312968	312738	312547	312288	310273
- 320668	313357	313293	313093	312863	312677	312418	310373
- 320868	313482	313418	313218	312988	312807	312548	310473
- 321068	313607	313543	313343	313113	312927	312668	310573
- 321268	313732	313668	313468	313238	313057	312798	310673
- 321468	313857	313793	313593	313363	313177	312918	310773
- 321668	313982	313918	313718	313488	313307	313048	310873
- 321868	314107	314043	313843	313613	313427	313168	310973
- 322068	314232	314168	313968	313738	313547	313288	311073
- 322268	314357	314293	314093	313863	313677	313418	311173
- 322468	314482	314418	314218	313988	313807	313548	311273
- 322668	314607	314543	314343	314113	313927	313668	311373
- 322868	314732	314668	314468	314238	314057	313798	311473
- 323068	314857	314793	314593	314363	314177	313918	311573
- 323268	314982	314918	314718	314488	314307	314048	311673
- 323468	315107	315043	314843	314613	314427	314168	311773
- 323668	315232	315168	314968	314738	314547	314288	311873
- 323868	315357	315293	315093	314863	314677	314418	311973
- 324068	315482	315418	315218	314988	314807	314548	312073
- 324268	315607	315543	315343	315113	314927	314668	312173
- 324468	315732	315668	315468	315238	315057	314798	312273
- 324668	315857	315793	315593	315363	315177	314918	312373
- 324868	315982	315918	315718	315488	315307	315048	312473
- 325068	316107	316043	315843	315613	315427	315168	312573
- 325268	316232	316168	315968	315738	315547	315288	312673
- 325468	316357	316293	316093	315863	315677	315418	312773
- 325668	316482	316418	316218	315988	315807	315548	312873
- 325868	316607	316543	316343	316113	315927	315668	312973
- 326068	316732	316668	316468	316			

The spectrograph used in this work was a 3.4 meter Ebert-type stigmatic instrument having a plane grating with 6000 lines/cm and 15 cm of ruling. The theoretical resolving power of the instrument is 100,000 with a linear dispersion of  $5 \text{ \AA}/\text{mm}$  in the first order. The critical slit width for the instrument is  $12\mu$  at  $5000 \text{ \AA}$ , which gives rise to very low instrumental line broadening and allows detailed examination of spectral line shapes. The arc was imaged on the slit with an achromatic lens. In addition, a Dove prism was used to rotate the arc image by 90 degrees, so that the arc axis was perpendicular to the entrance slit of the spectrograph. All of the work being reported here was done photographically, with the optical density of the spectral plates recorded by a scanning microdensitometer. A standard tungsten strip lamp and rotating sector were used for photographic plate calibration.

Self-absorption in the arc plasma was checked by using a concave mirror to reflect some of the light of the arc back through the arc a second time. Additivity of intensities indicates the absence of self-absorption, and this method provides a simple, convenient check for such absorption.

## 2.6 SPECTROSCOPIC TEMPERATURE MEASUREMENTS

### 2.6.1 Argon

Since temperatures and degrees of excitation were previously unknown in our arc, a survey of all argon spectral lines in the visible and near infrared was made initially for purposes of line identification and to qualitatively estimate intensity ratios within these lines. Fifteen atomic lines with known transition probabilities were

identified in the region  $\lambda 6500$  to  $\lambda 9000 \text{ \AA}$  and two ionic lines with known transition probabilities in the region  $\lambda 3700$  to  $\lambda 4300 \text{ \AA}$ . No impurity lines were definitely observed. An electron continuum was apparent in a portion of the spectral region.

Of the choices available for measuring the temperature of the argon arc, the radial intensity inversion technique was chosen as being most appropriate. The discussion in section 2.7 will demonstrate that some uncertainty may exist in the transition probability data and thus possibly invalidate temperatures which would be obtained by using line intensity ratios.

The  $\lambda 8264$  argon line, after being tested for self-absorption, was chosen for the temperature measurements. The energy of the upper energy state giving rise to this transition is 13.3 ev. A plot of the intensity-temperature distribution of this  $\lambda 8264$  line (as computed by using the atom number densities and the Boltzmann factor) is given in Figure 12. As can be seen, the temperature for which the intensity of this line is a maximum is approximately  $15,300^\circ\text{K}$ . Thus, if the plasma temperature on the axis of the arc exceeds this value, a distribution of the intensity of this line as a function of arc radius will exhibit a maximum, which corresponds precisely to a temperature of  $15,300^\circ\text{K}$ . Once this point is established, a complete radial temperature profile can be easily established by comparing the relative intensities as a function of temperature in Figure 12 to the relative intensities as a function of arc radius as obtained spectrographically.

It was found, after several trials, that an argon arc operating at 270 amps showed a pronounced off-axis intensity peak. The data were obtained with the spectrographic slit optically aligned

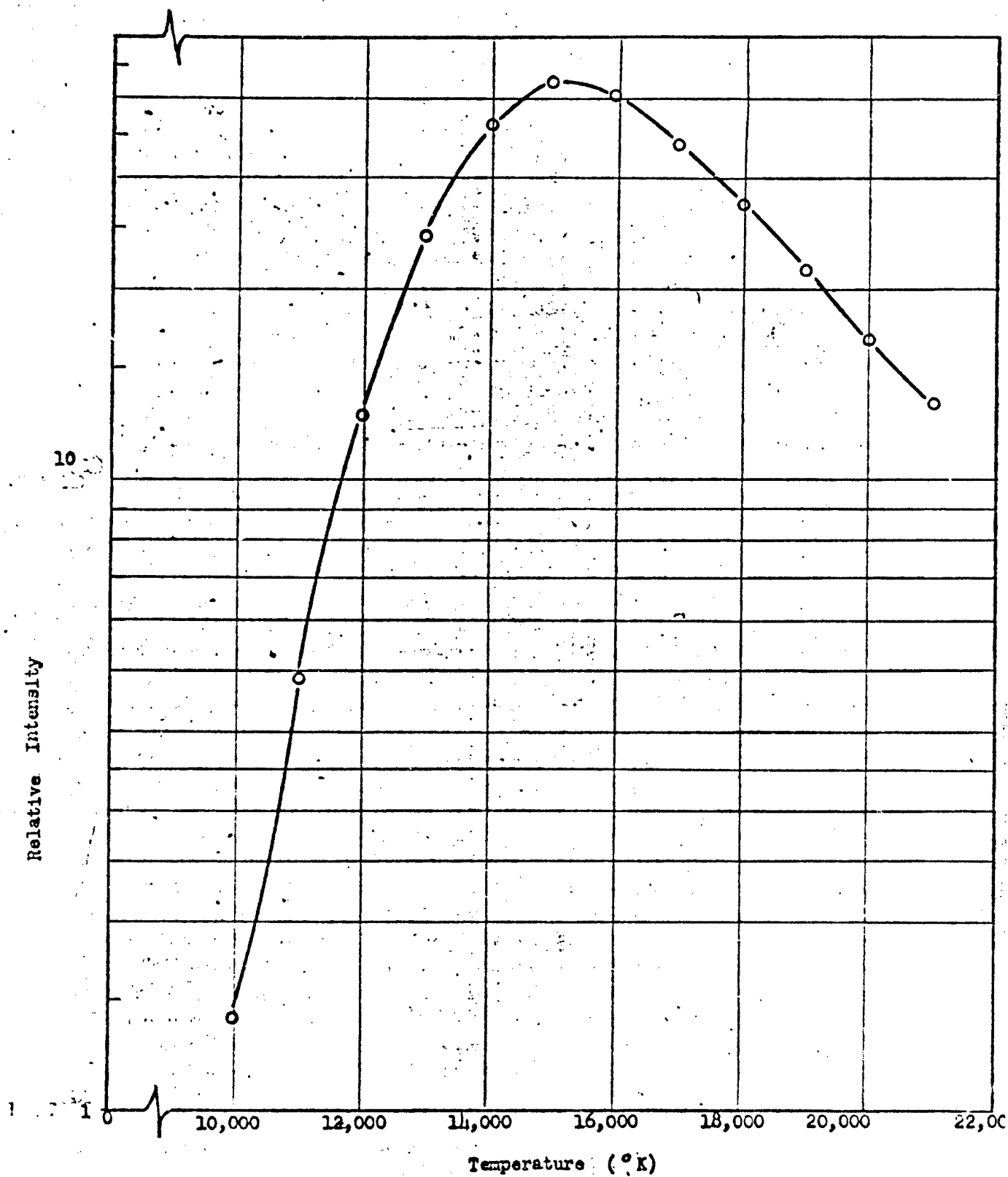


FIG. 12 CALCULATED INTENSITY-TEMPERATURE DISTRIBUTION OF THE ATOMIC  $\lambda 8264$  SPECTRAL LINE IN ARGON.



transverse to the arc itself, so that the height of any spectral line as it appeared on the photographic plate corresponds to a radial view of the arc at a distance of several millimeters above the anode in a 3/8-inch long arc. A 200 $\mu$  entrance slit width was used with exposure times varying from 1/100 to 1/5 of a second. A microdensitometer record of the intensity versus height along the spectral line provided a measure of the intensity as a function of transverse distance across the arc. Using the Abel integral equation and the coefficients given in Table 1, a measure of the intensity versus arc radial distance was obtained. Converting this information to temperature (using Figure 12) resulted in the radial temperature distribution for the argon arc as given in Figure 13.

#### 2.6.2 Helium

The problem of measuring temperatures in a helium plasma proved considerably more difficult than originally anticipated. First of all, the only transition probability data in the visible exist for spectral lines with upper energy states between 21 and 23 ev. This narrow range scarcely provides the sensitivity required for using line intensity ratios. This method could be used if one could get down to the 600  $\text{\AA}$  region or use an ionic line. However, we were not equipped to do spectroscopy in the ultraviolet, and no ionic lines were observed in our spectra.

However, since we had data on helium plasma composition and spectral line broadening [18, 19], and since our spectrograph had sufficient dispersion and resolution to examine line shapes, we considered the procedure for relating line broadening to electron density and temperature. The best diagnostic spectral lines appeared to be the

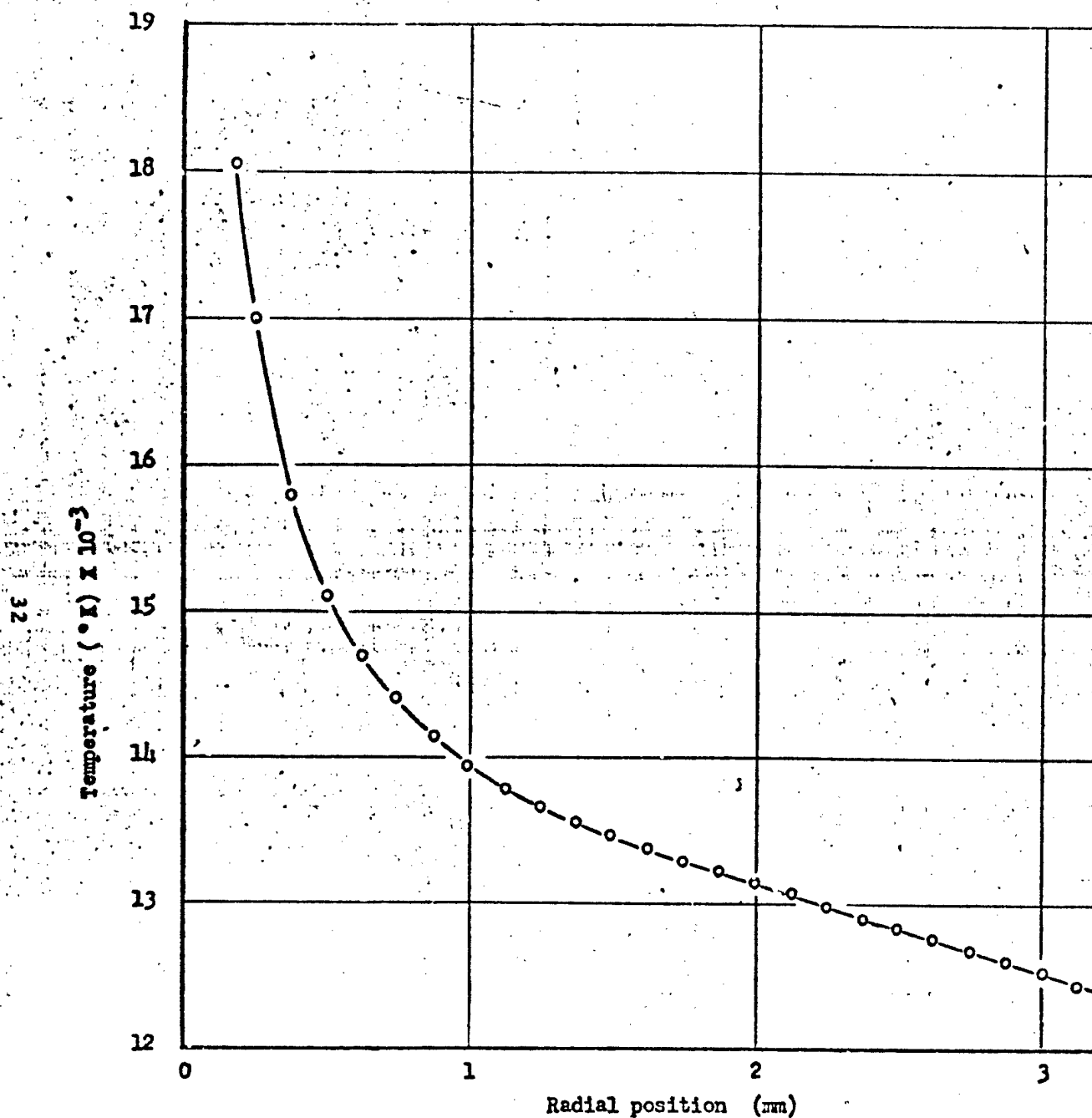
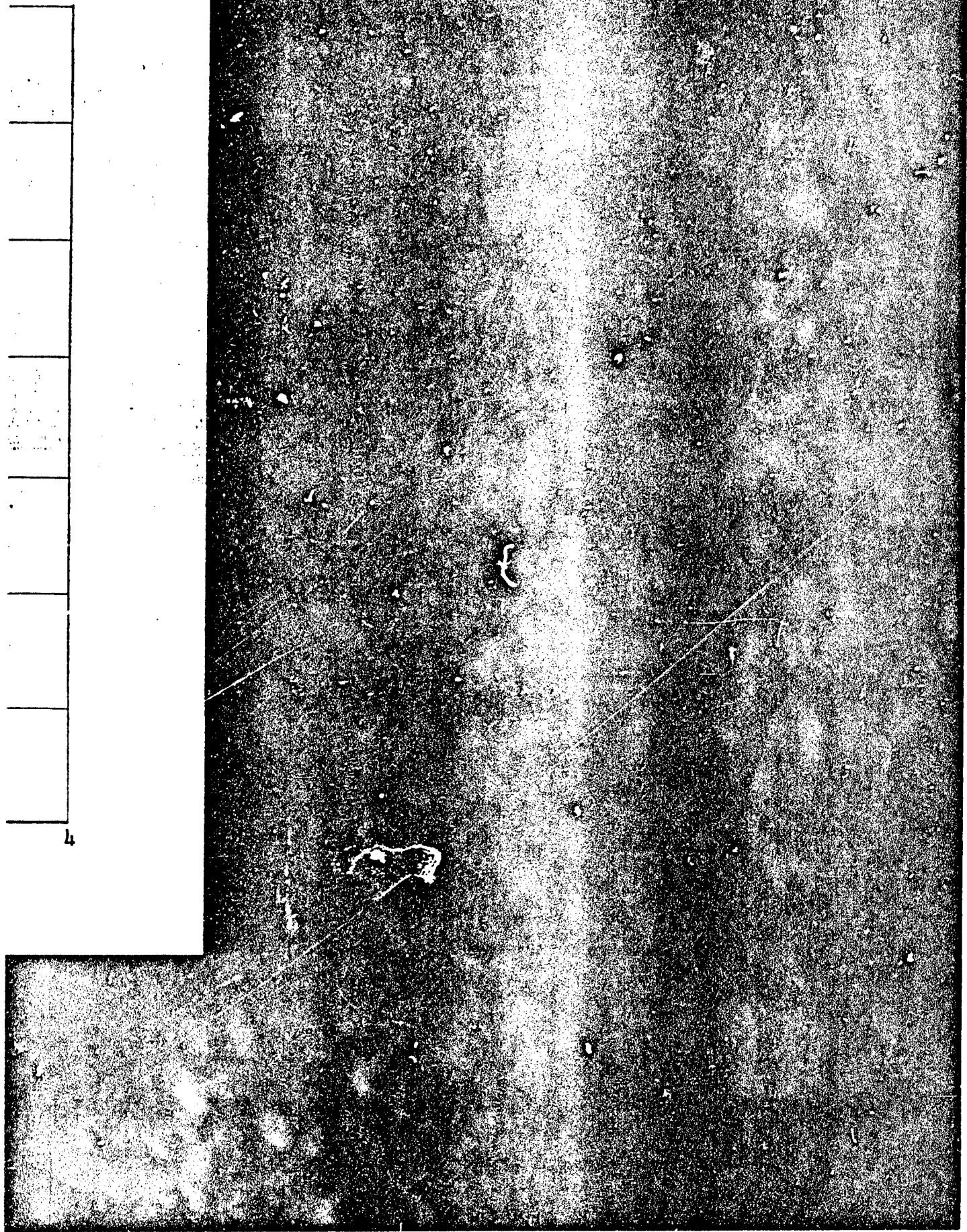


FIG. 13 TEMPERATURE vs RADIUS IN A 270-AMPERE ARGON ARC ABOVE ANOD



B

$\lambda 5015$  and  $\lambda 4713$ , since they both have fairly large shifts and widths, are approximately symmetrical in wavelength, and are reasonably strong lines.

After considerable preliminary work, observations were made of the  $\lambda 5015$  line using the second order dispersion for an arc current of 230 amps. A 10-micron entrance slit was used, and again a transverse view of the arc above the anode was exposed along the length of the slit. After plate exposure and processing, a fine line, parallel to the spectral lines, was scribed on the plate to provide a reference from which wavelengths corresponding to the spectral line originating from different parts of the arc could be accurately correlated. In this way, line shifts as well as widths could be determined as a function of arc radius. Once again, of course, the Abel inversion process was required to correct the observed transverse intensity to a true radial intensity.

The theory used was that of Griem, which had been confirmed experimentally by Berg [23], and which relates the electron density in a helium plasma to the width and wavelength shift of the neutral helium spectral lines, even in the absence of LTE. In this theory, the width at half-height and the wavelength shift of the line peak are linear functions of the electron density and vary only slightly with electron temperature. For the  $\lambda 5015$  line, the electron density  $n_e = 1.14 \times 10^{16} \Delta \lambda_{1/2}$ , where  $\Delta \lambda_{1/2}$  is the full width at half-maximum in angstroms, and  $n_e = 3.89 \times 10^{16} \Delta \lambda$ , where  $\Delta \lambda$  is the wavelength shift of the intensity maximum in angstroms.

Examination of the data revealed that our half-width measurements appeared consistent and reliable but that the wavelength shift measurements were unsatisfactory due to the inability of our

microdensitometer-recorder system to accurately determine absolute wavelength. The half-width data, then, provided electron density which was converted to temperature by the use of Saha's equation. As it turned out, a temperature variation of less than  $1000^{\circ}\text{K}$  was measured across the portion of the arc which was exposed spectrographically. Since time did not permit the rather extensive data reduction procedure which would have been required for additional exposures of the helium arc, data for this gas is given only for a temperature of  $15,000^{\circ}\text{K}$  (that measured by the line-broadening technique).

### 2.6.3 Nitrogen

As described above, nitrogen gas was mixed with argon to provide an atmosphere in which electrode erosion could be eliminated. The arc was operated with the nitrogen component as large as possible (commensurate with this electrode condition) to provide maximum sensitivity when comparing properties of this argon-nitrogen arc to the pure argon arc.

After variations of gas ratios and arc current had been investigated, spectral plates were exposed using an arc current of 350 amps with a gas ratio of 66 per cent argon, 34 per cent nitrogen. As in the case of pure argon, a 200-micron entrance slit width was used with exposure times between  $1/100$  and  $1/10$  of a second. Also the  $\lambda 8264$  line in argon was once again used for the temperature determination with a correction being made for the change in argon atom density as a function of temperature. Using the same process of applying Able's integral equation and transforming the observed transverse intensity to a true radial intensity, the temperature versus arc radius distribution shown in Figure 14 was obtained.

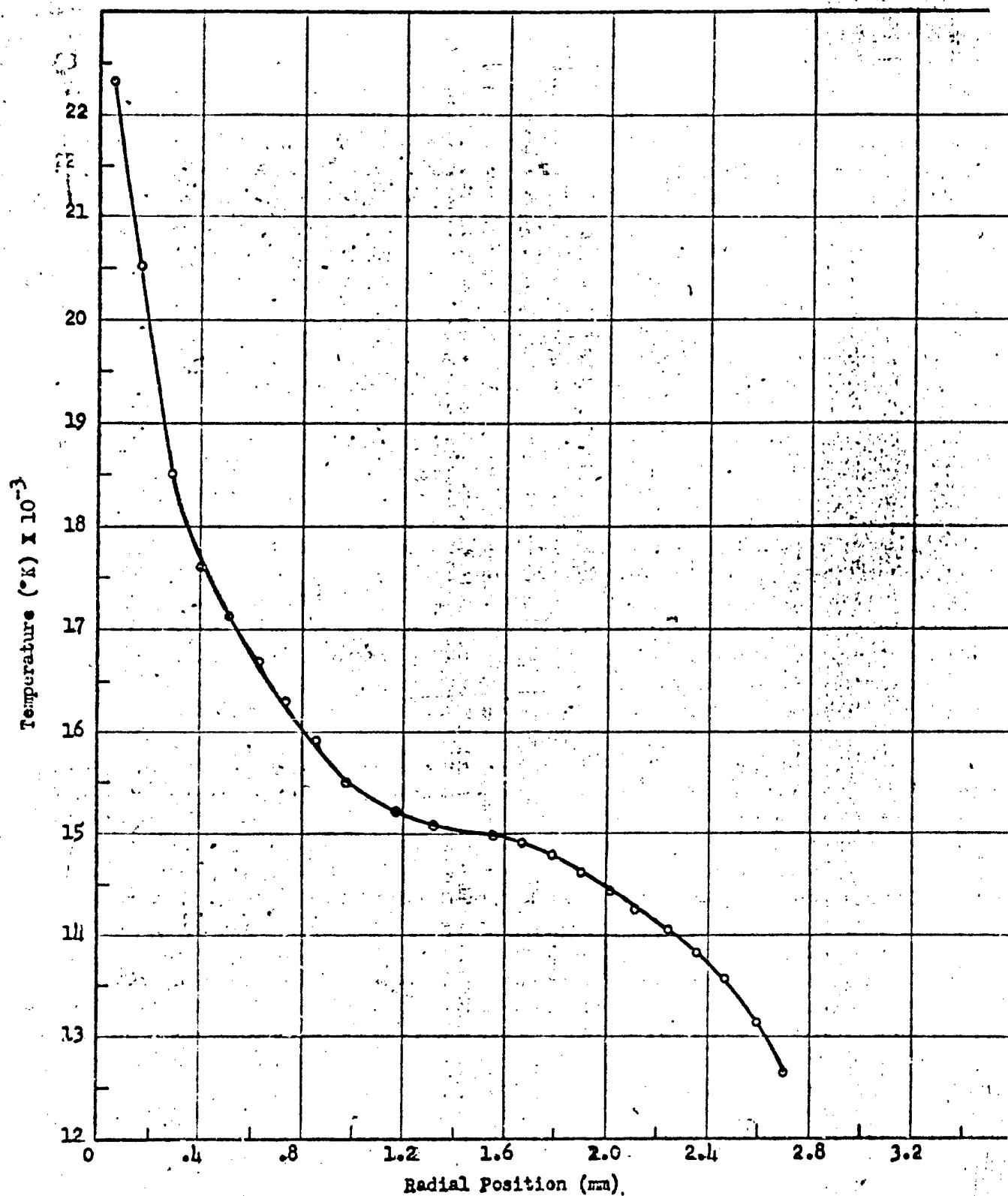


FIG. 11. TEMPERATURE vs. RADIUS IN 350-AMPERE,, 34% NITROGEN, 66% ARGON ARC ABOVE ANODE SURFACE.

## 2.7 SPECTRAL LINE SHAPES IN ARGON

Quite unexpectedly, a seemingly curious condition was found to exist concerning the shapes of atomic argon spectral lines. Of the fifteen lines in the region  $\lambda 6500$  to  $\lambda 9000 \text{ \AA}$ , several show a strong shift of the intensity peak to the red along with a pronounced dip on the blue side of the line, while others are relatively unaffected. A typical example of a line exhibiting such characteristics is shown in Figure 15. The slit width used here was 10 microns, providing an instrumental line width of less than  $0.05 \text{ \AA}$ . This condition is not present at arc currents of 50 amps, begins to appear between 100 and 200 amps, and is fully developed at 250 amps. Although this situation did not affect our measurements, it is of some interest for its own sake. It is mentioned here for the sake of completeness and to make it more generally known to workers in the field.

It initially seemed strange that some lines were affected and others not, since all of the lines mentioned have about the same upper energy state ( $\approx 13 \text{ ev}$ ) and about the same lower energy state ( $\approx 11 \text{ ev}$ ) and, further, there exists no correlation with the atomic configurations of the energy states giving rise to these transitions. There was further no correlation between the affect and the latest published values for argon transition probabilities [16].

A literature search was made at this point, and it became apparent that there were many instances of argon lines being shifted rather strongly to the red. This shift is in general caused by the interaction of the emitting atom with the surrounding charges in the plasma and is directly proportional to the electron density. This explains the dependence of the line profile on the current, since the electron

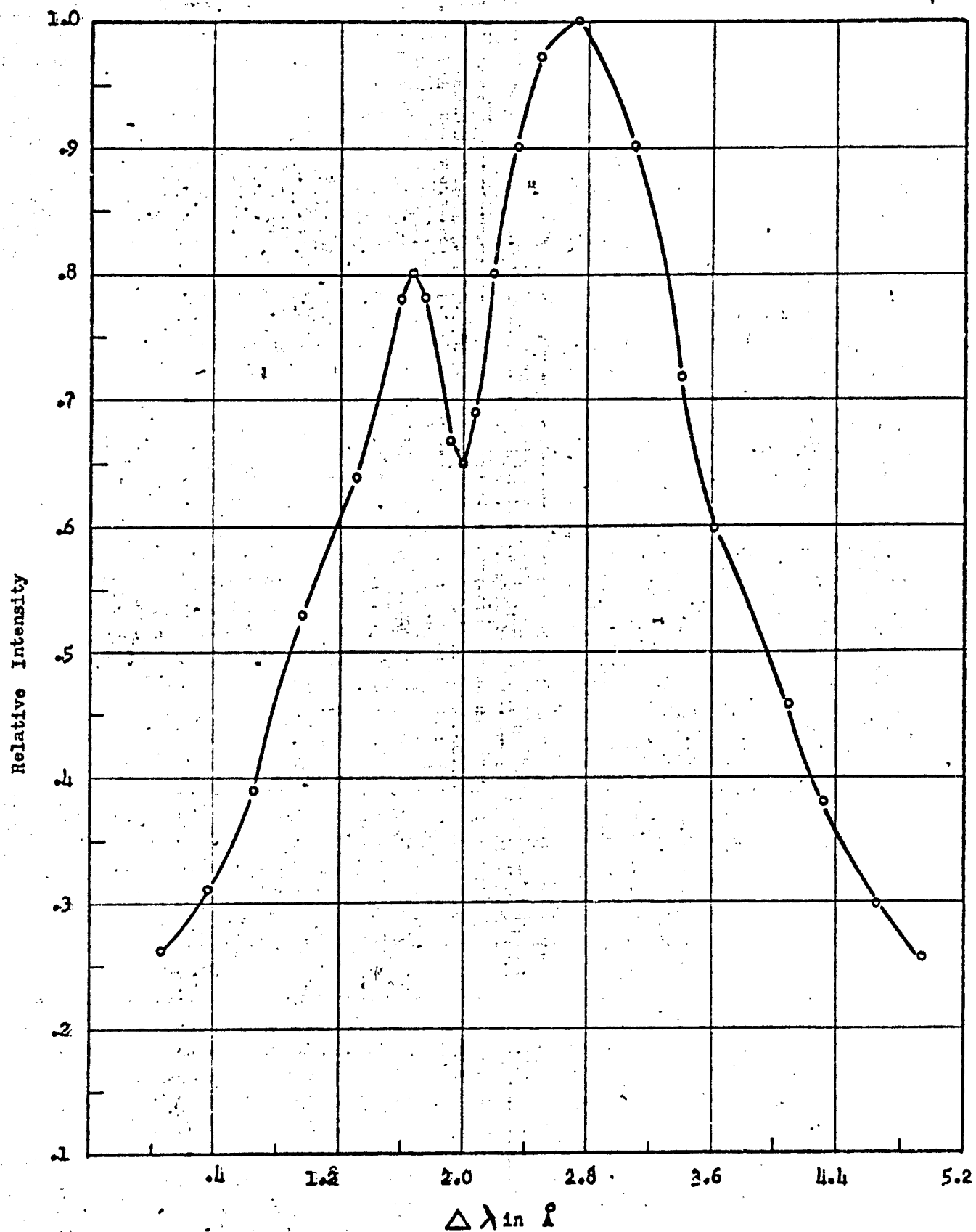


FIG. 15 PROFILE OF THE  $\lambda 8115$  LINE IN AN ARGON ARC AT 200 AMPERES



density depends on the arc current. The dip in the curve has been assumed to be due to absorption of radiation in cooler layers surrounding the hottest part of the arc. A calculation of the radiation flux from the axis of the arc through the absorbing layer suggests that absorption can be appreciable if the absorbing layer is about 1 mm in thickness. It is strange that absorption should occur from a level lying more than 11 volts above the ground state, but calculations also show that this is possible.

In the case that absorption is actually responsible for the dip in the lines, those lines with larger transition probabilities should be absorbed more strongly. It has been mentioned here that no such correlation was observed with the latest values for transition probabilities. However, previous values [24] do show a good correlation, so the possibility exists that these initial values are actually the correct ones and later values may be in error. More work should be done to substantiate this inference based on these line broadening observations.

One further interesting point is that some crude approximations were made using our line profiles and the only data [25] found in the literature which was applicable. The shift in the intensity peak of the  $\lambda 8115$  line corresponds roughly to an electron density of about  $1.7 \times 10^{17}/\text{cm}^3$ , or a temperature of about  $15,000^\circ\text{K}$ . The shift of the intensity dip indicates the absorbing layer was at a temperature of about  $11,000^\circ\text{K}$ . These temperatures are in agreement with those obtained by the intensity inversion of the  $\lambda 8264$  line as shown in Figure 12.

## 2.8 ELECTRIC FIELD DETERMINATIONS

The electric field in the arc plasma was determined for each particular case of interest by measuring the total voltage across the arc and subtracting from this the sum of the electrode drops. The electrode drops in an atmospheric pressure arc can be determined with reasonable accuracy by plotting the total arc voltage as a function of arc length and then extrapolating the curve back to zero length. The point where the curve intercepts the voltage axis is then the sum of the anode and cathode drops. Data for the three gases are given in Figures 16, 17, and 18 for the arc currents at which spectroscopic data were obtained in each case.

## 2.9 RADIAL CURRENT DENSITY DISTRIBUTIONS

In order to measure current densities as a function of arc radius, a special anode was fabricated with a probe inserted directly at the center (see Figure 19). This probe, 0.040 inch in diameter, is mounted in a conventional anode plate and insulated from the rest of the structure so that fractional amounts of current to the probe and the anode surface can be measured.

In its design, one has to consider such problems as resolution, electrical insulation, and cooling. The probe tip must be of small diameter to insure that a great number of readings can be taken over the total diameter of the arc. Good resolution is necessitated by the fact that values of current density may change by three orders of magnitude within a radial increment of 2 mm.

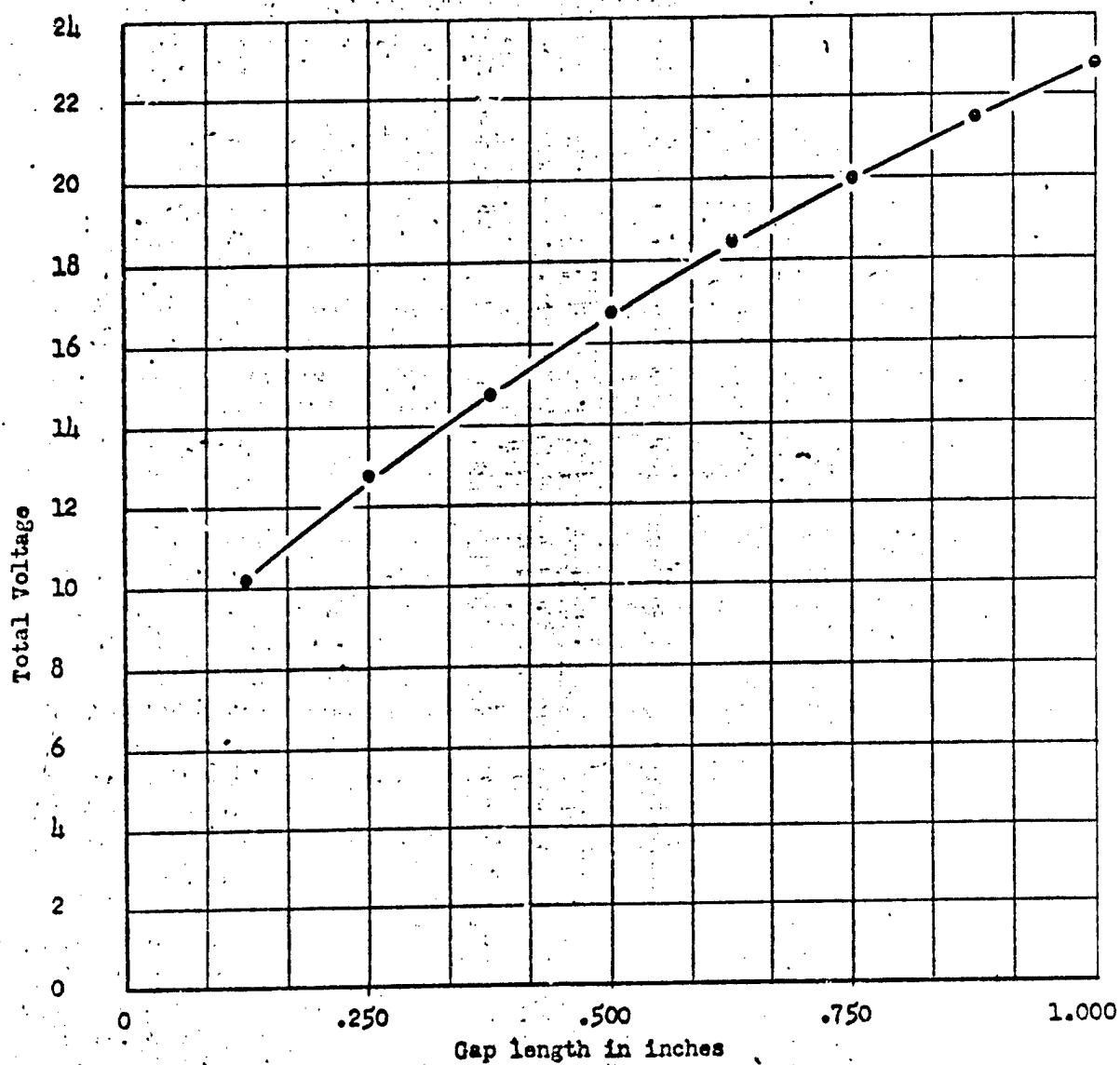


FIG. 16 ARC VOLTAGE vs LENGTH FOR 270 AMPERES IN ARGON

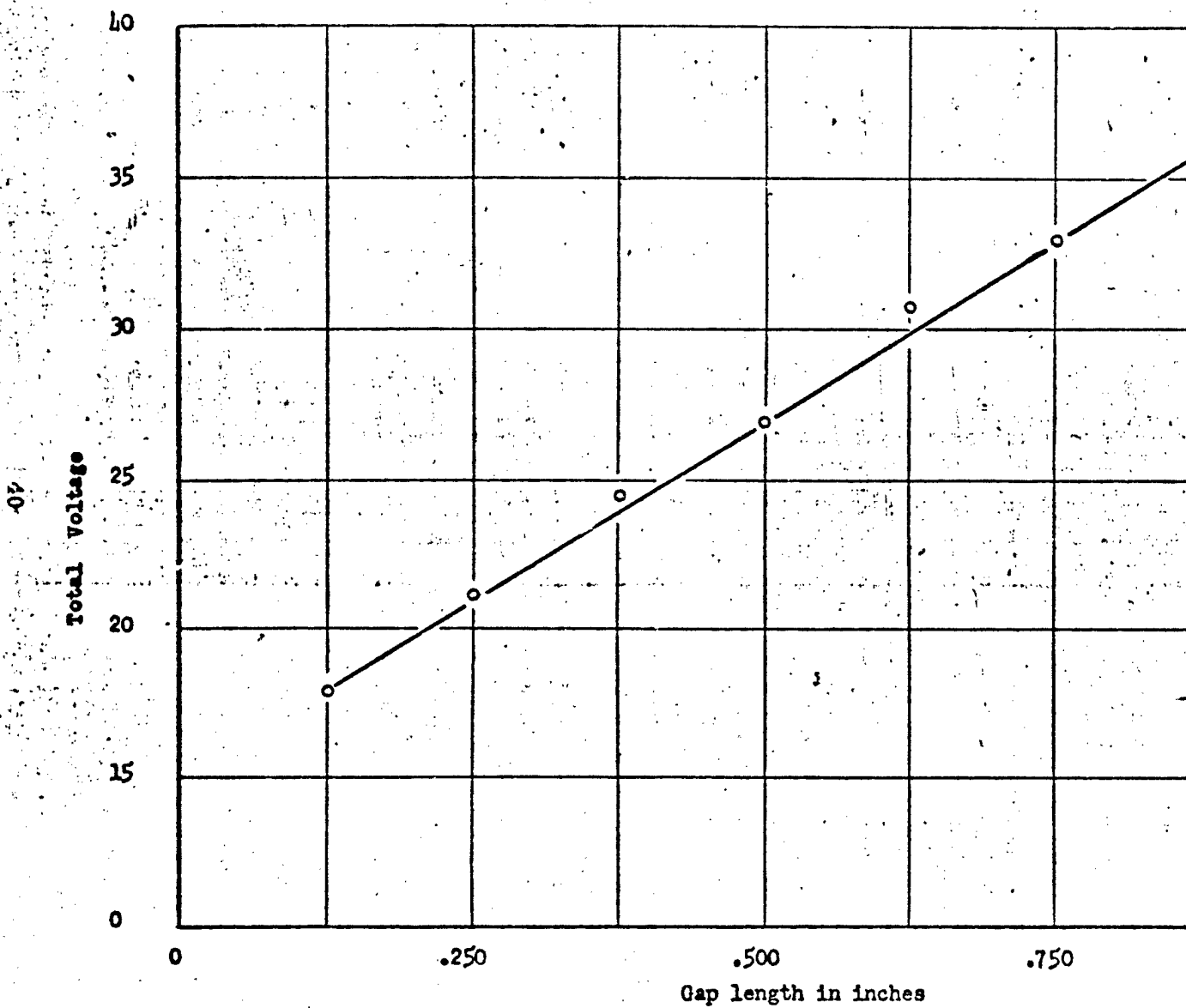
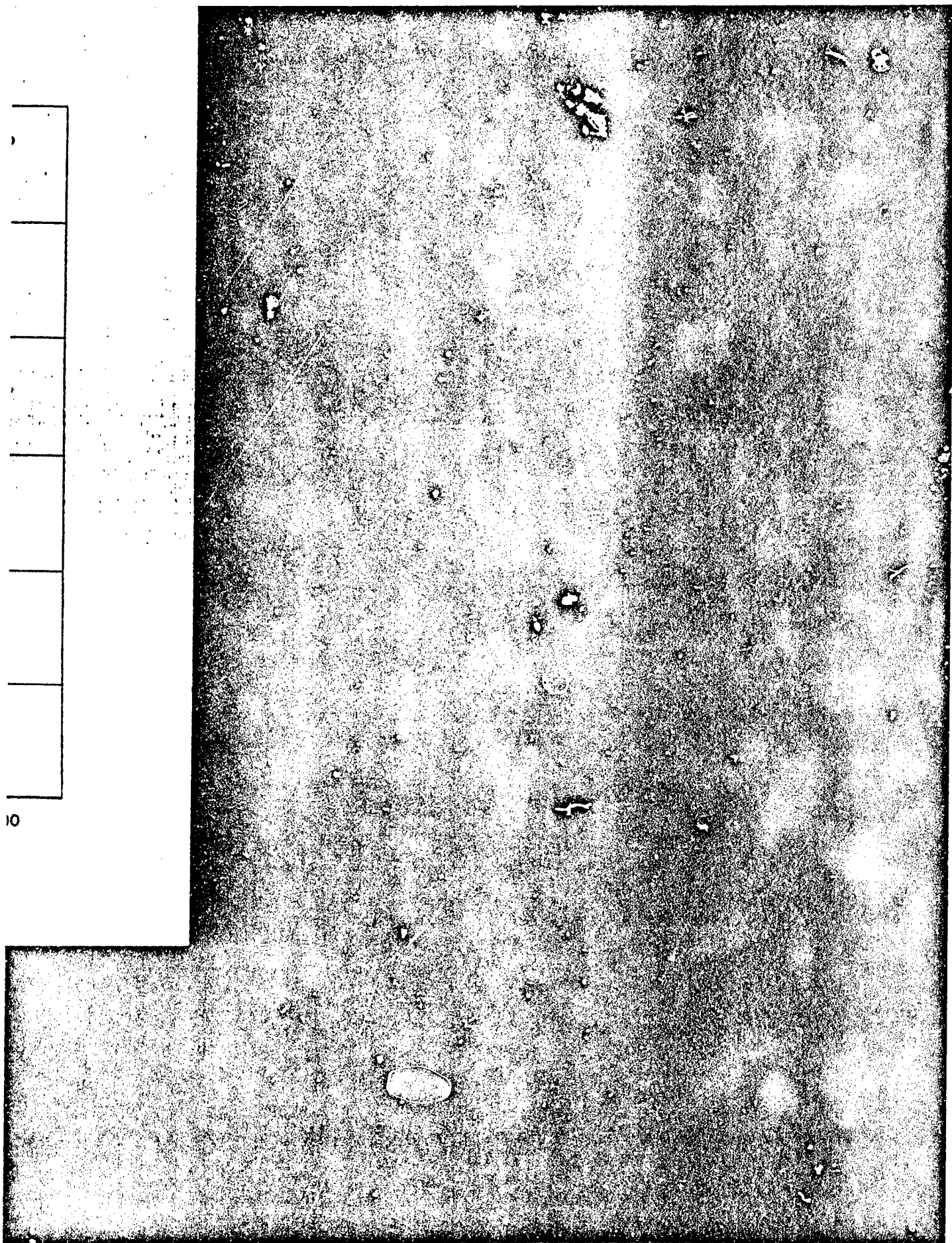


FIG. 17 ARC VOLTAGE vs. LENGTH FOR 230 AMPERES IN HELIUM



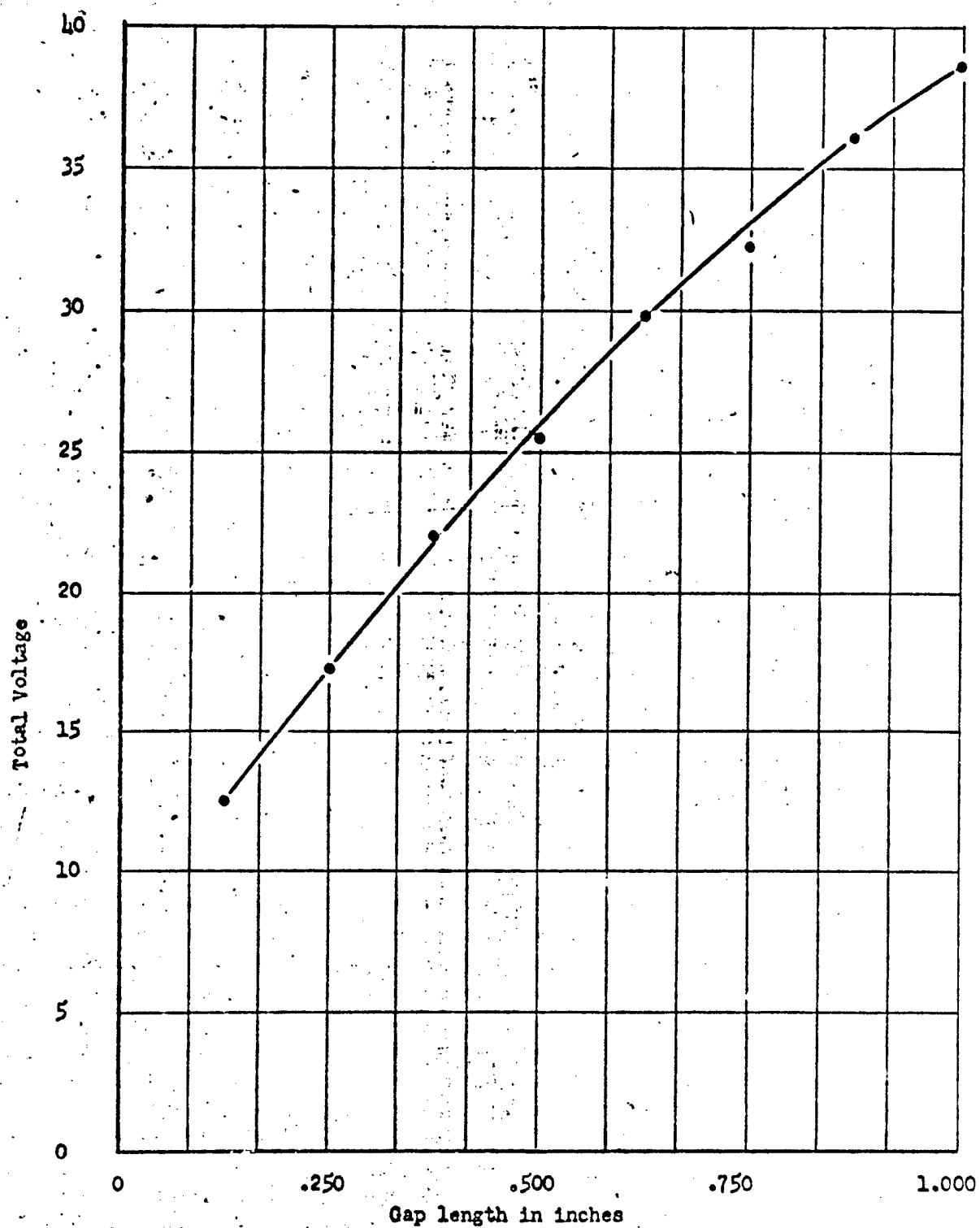


FIG. 18 ARC VOLTAGE vs LENGTH FOR 350 AMPERES IN 66% ARGON, 34% NITROGEN

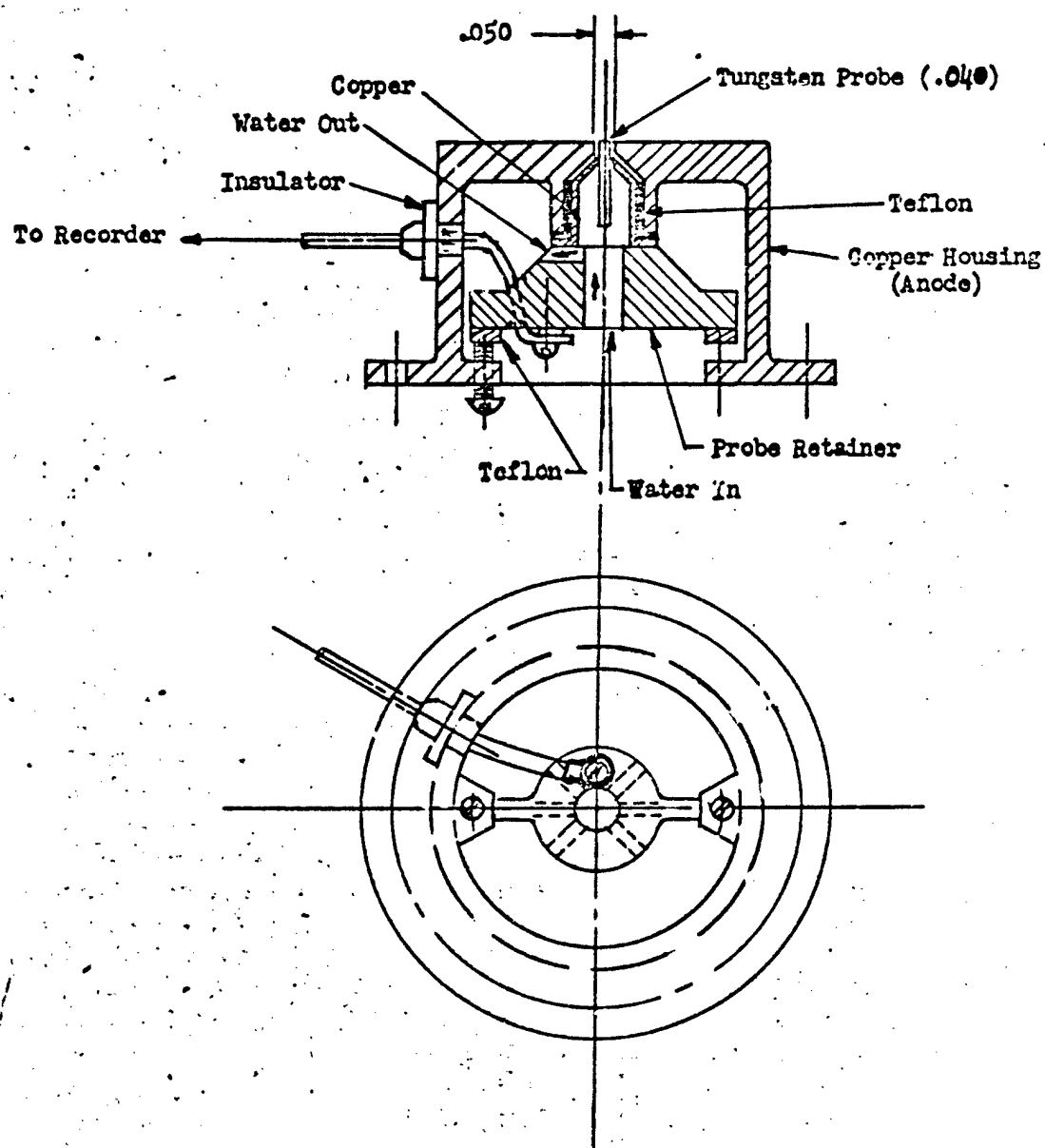


FIG. 19 SCHEMATIC OF THE CURRENT PROBE-ANODE

Since the probe tip must be electrically insulated from the rest of the anode, its assembly alone must conduct the heat to the cooling water below. At the center of symmetry of the arc, the current density is a maximum, and probe diameter must be of sufficient diameter to thermally conduct the heat generated at the surface of the probe as well as the joule heat generated within the probe by the high current densities. Consequently, the probe tip was made as short as possible and was fitted into a copper cone which presented a much larger area to the cooling water than could the probe tip alone.

While the probe tip and the rest of the anode are not electrically connected by a metal, they are connected by the cooling water. However, since both tip and rest of the anode are at the same potential, except for second order inhomogeneities in the field, the leakage current between the two is extremely small and completely negligible.

By moving the entire anode structure in a direction transverse to the arc column, the probe measures current as a function of arc radius, which can easily be transformed to current density. Data were always checked by integrating the current density curve thus obtained and comparing it with an independent total current measurement.

Figure 19 shows that the anode cooling water may be expected to be as effective as in the case of the regular anode, except in a small region immediately surrounding the probe. Initial testing of the unit showed perfectly satisfactory operation in helium and argon arcs, with no erosion occurring at either the probe or the rest of the anode surface. To obtain data, then, the anode was simply cranked by hand across the arc, and probe current was read using a series of ammeters (see Figure 20a



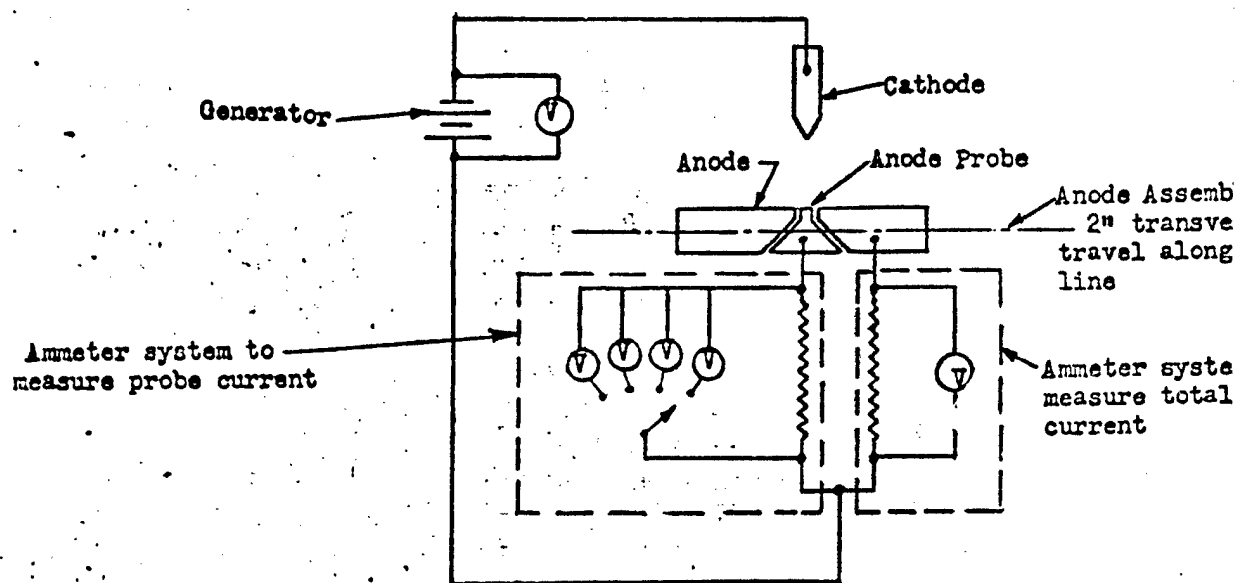


FIG. 20(a) CIRCUITRY USED WITH CURRENT PROBE-ANODE IN ARGON AND HELIUM

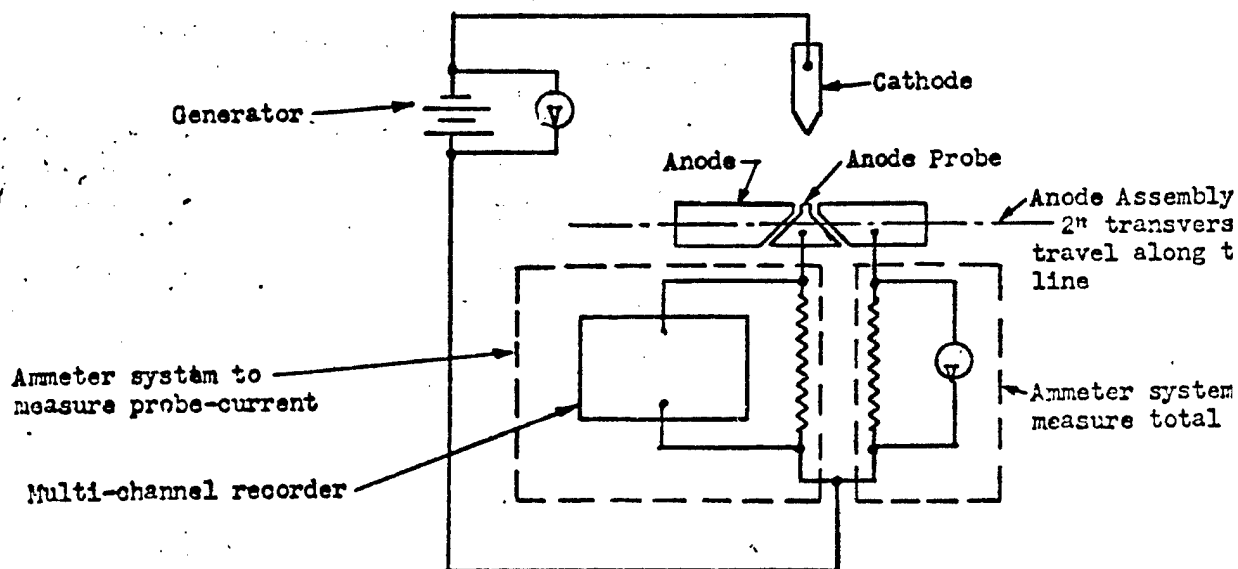


FIG. 21(b) CIRCUITRY USED WITH CURRENT PROBE-ANODE IN NITROGEN-ARGON MIXTURE

However, for the case of the argon-nitrogen arc, the effect of the higher current (350 amperes versus 270 or 230 amperes) along with the deleterious effect of nitrogen on electrode surfaces resulted in a series of failures due to erosion in the immediate vicinity of the probe. This situation was remedied by using an electric motor-gear box assembly which moved the anode across the arc at a rate of 5 inches/minute. The time the probe spent near or in the hot central portion of the arc was thus much reduced, and no erosion occurred. A multi-channel recorder was used in this case to record the probe current as a function of arc radius (see Figure 20b). Current densities measured with this technique are shown in Figures 21, 22, and 23 for argon, helium, and argon-nitrogen, respectively.

### 3. RESULTS

#### 3.1 CROSS SECTIONS

Equation (8) in section 2.2 forms the basis for our atom-electron cross section determinations. Rewriting this expression, we have that the atom-electron collision cross section  $Q_e^a$  is given by the relation

$$Q_e^a = \frac{1}{n_a} \left\{ \frac{e^2}{\left(\frac{8mK}{\pi}\right)^{1/2}} \frac{n_e E}{J T^{1/2}} - n_i Q_e^i \right\} \quad (17)$$

We have seen in the previous discussion how the electric field  $E$ , the current density  $J$ , and the temperature  $T$  were experimentally measured in arcs operating in argon, helium, and a known mixture of argon and nitrogen. Further, the electron, ion, and atom number densities

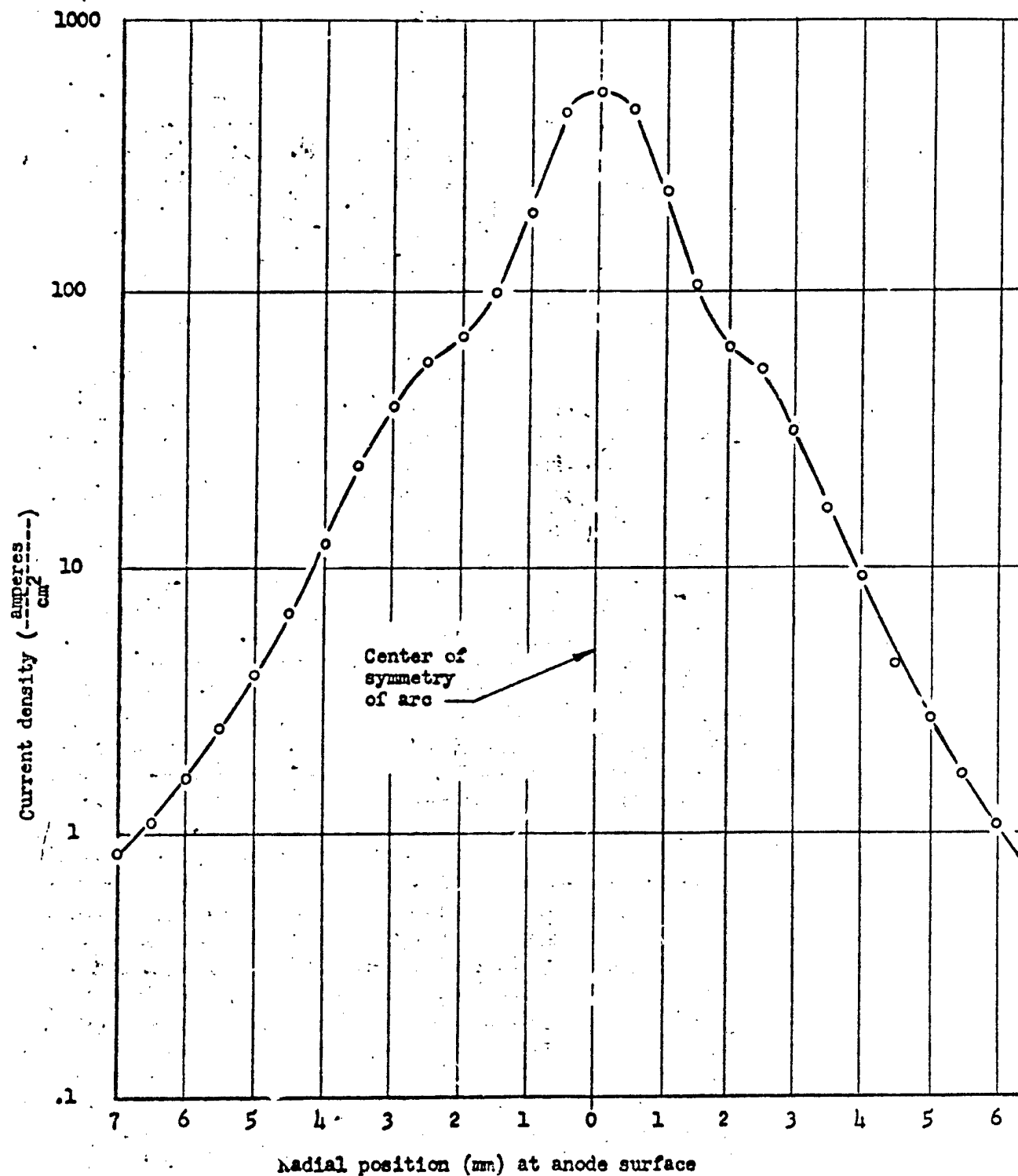


FIG. 21 CURRENT DENSITY vs ARC RADIUS IN AN ARGON ARC AT 270 AMPERES

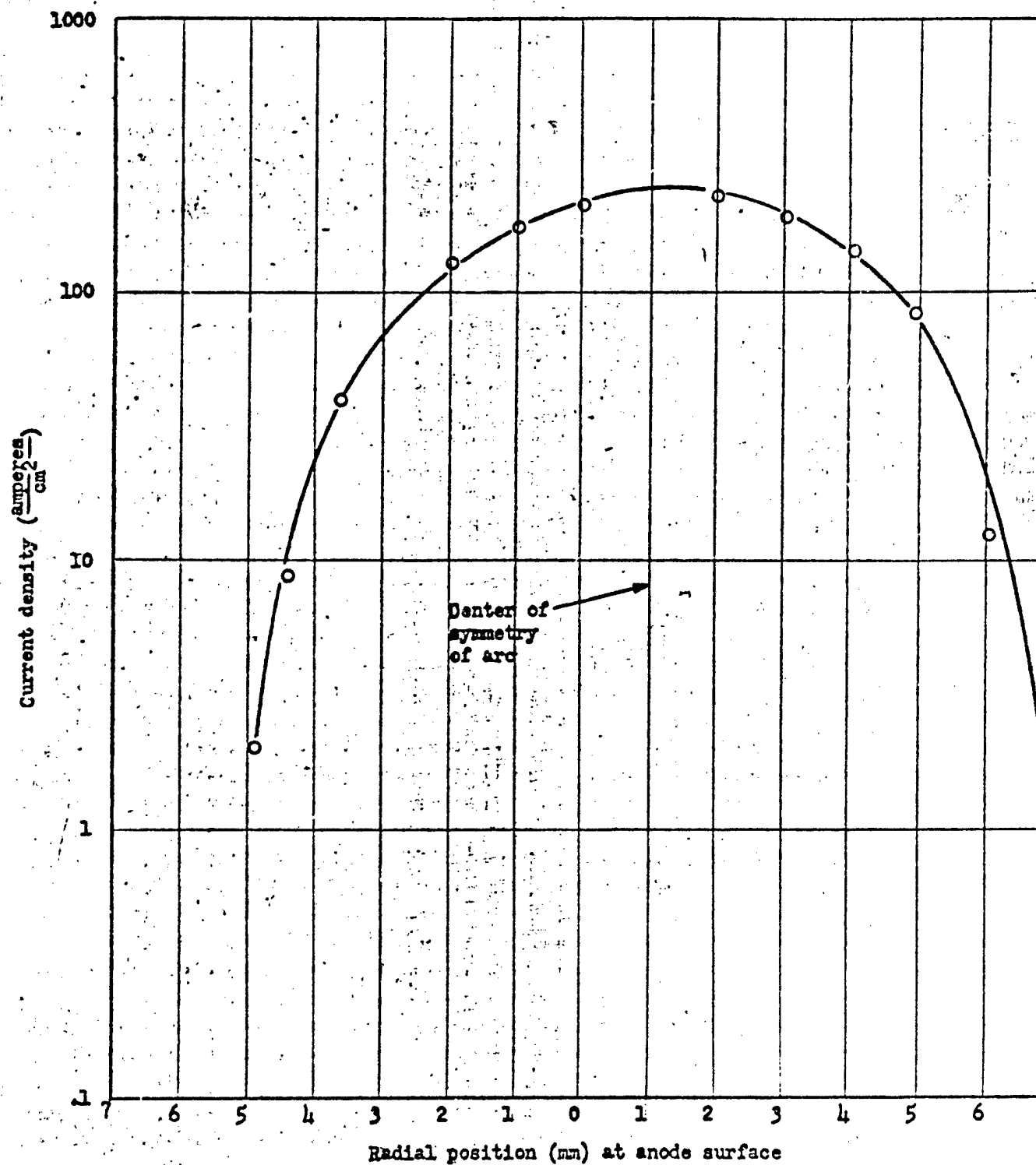


FIG. 22 CURRENT DENSITY vs ARC RADIUS IN HELIUM ARC  
at 230 AMPERES

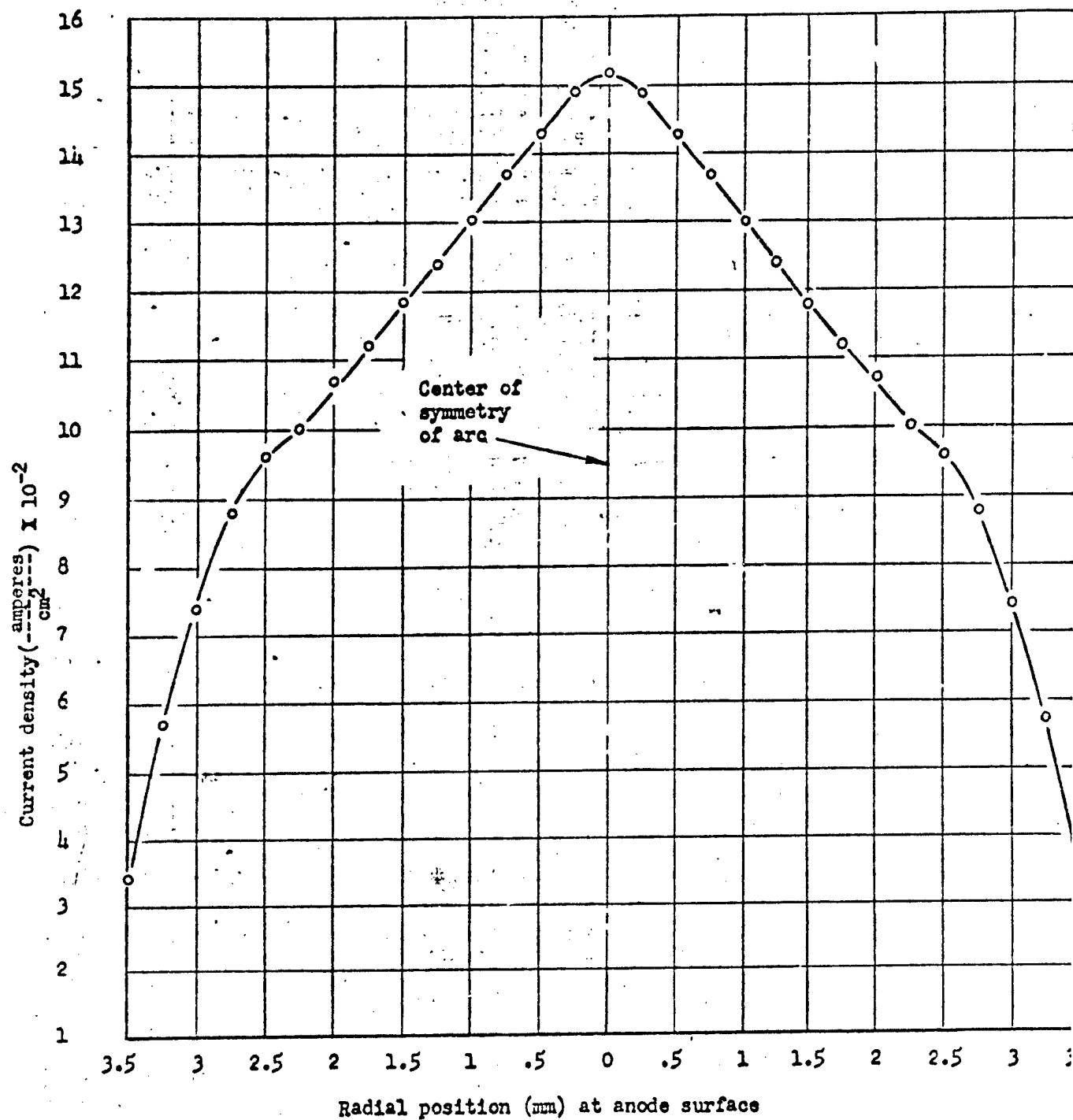


FIG. 23 CURRENT DENSITY vs ARC RADIUS IN AN ARGON -- NITROGEN ARC AT 350 AMPERES

( $n_e$ ,  $n_i$ , and  $n_a$ , respectively) as well as the ion-electron cross sections  $Q_e^i$  were all computed as functions of temperature for the gases of interest. The cross sections can therefore be computed as functions of temperature over a range which was determined spectroscopically for each particular gas. Even though the correction was small, the presence of doubly charged ions was included in the term ( $n_i Q_e^i$ ) on the R. H. S. of Eq. (17).

Values obtained in this manner for cross sections in argon are shown in Figure 24. Making use of these values for argon and the known gas percentages in the argon-nitrogen arc, and writing the terms involving cross sections in Eq. (17) as sums over both argon and nitrogen contributions, cross sections for nitrogen can be obtained. These are given in Figure 25. Finally, for the case of helium, temperatures in the arc were measured only at positions which corresponded very nearly to 15,000°K. Therefore, the cross section was evaluated only at 15,000°K for helium and was found to be  $2.09 \times 10^{-15} \text{ cm}^2$ .

At first sight, these cross sections seem somewhat larger than what may have been expected. However, recent theoretical work has raised estimates of these values by an order of magnitude or more for the temperature range under consideration here. For example, a straightforward use of the Born approximation for hydrogen yields a value of  $3.5 \times 10^{-16} \text{ cm}^2$  for the atom-electron collision cross section. Quantum mechanical calculations by Mower [26] and Massey and Morseiwitsch [27], on the other hand, increased this value to  $25 \times 10^{-16} \text{ cm}^2$ . This latter value is in keeping with those obtained in our experiments.

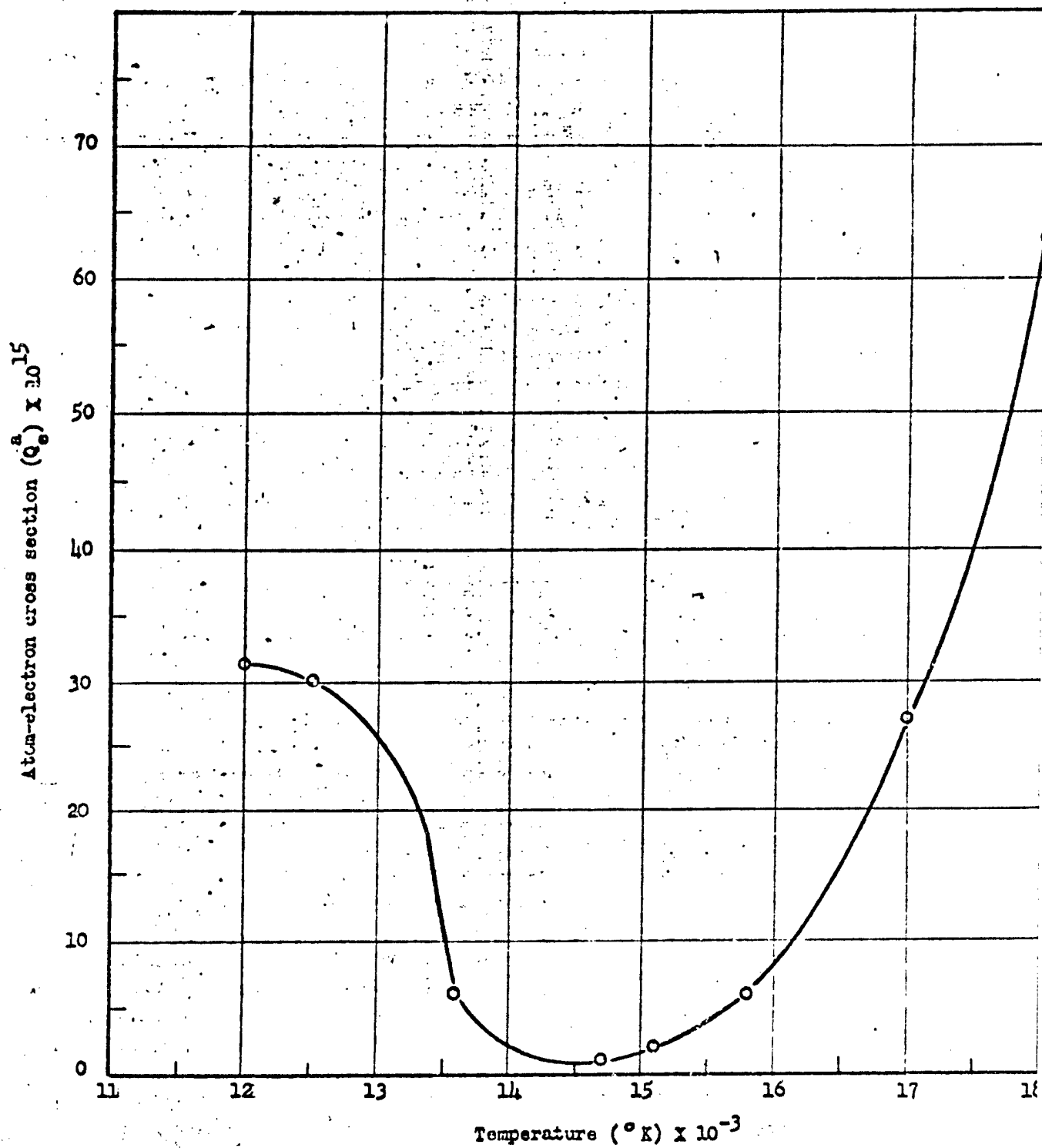


FIG. 24. ATOM-ELECTRON COLLISION CROSS-SECTIONS IN ARGON

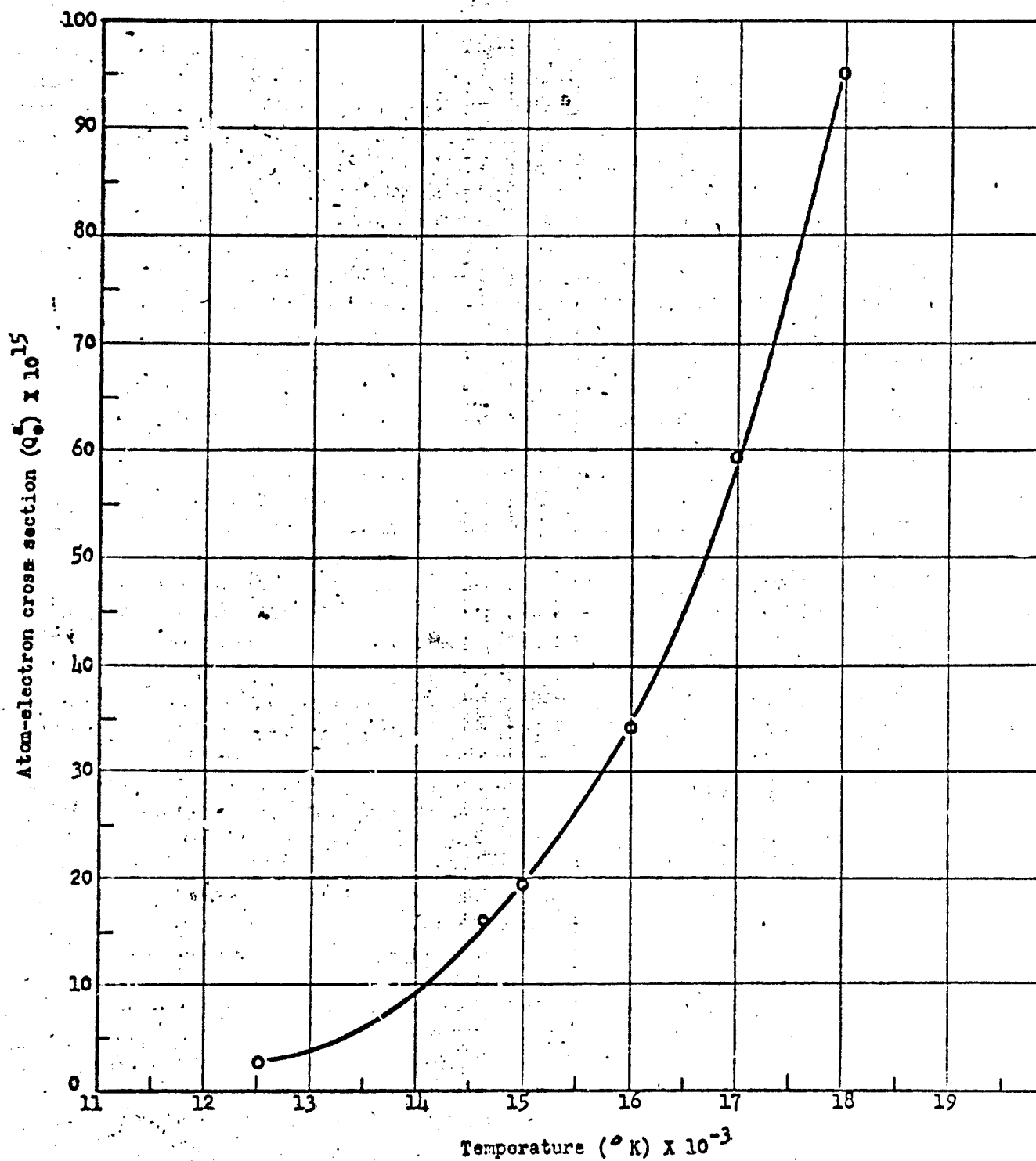


FIG. 2: ATOM-ELECTRON COLLISIONS CROSS SECTIONS IN NITROGEN



It should be mentioned here that results of previous work at higher energies have often been expressed in terms of a collision probability. This quantity is really the absorption coefficient divided by the gas pressure and is expressed in units of  $(\text{cm} - \text{mm Hg})^{-1}$ . Any such numbers can be converted to cross sections as given in this report upon multiplication by the numerical factor  $2.81 \times 10^{-17}$ .

### 3.2 TRANSPORT PROPERTIES

The measurable physical quantities in the arc columns (electric field, current density, temperature) were used to compute collision cross sections for argon, helium, and nitrogen. We shall now attempt to use the values for these cross sections in estimating certain transport properties for these gases.

To illustrate what must be done, we recall, for example, that the dynamical viscosity of a gas is given as

$$\eta = \frac{1}{3} n m \lambda \bar{v} . \quad (18)$$

In this formula,  $\bar{v}$  is the mean velocity of the atoms or molecules,  $\lambda$  is the mean free path,  $m$  is the mass, and  $n$  is the number density of the particles. Under normal conditions, the factor  $n$  can be eliminated using the relation  $\lambda = 1/nQ$ , where  $Q$  is the effective collision cross section. This shows that such properties as the viscosity are normally independent of pressure. However, with increasing temperature a certain portion of the gas becomes ionized. The properties of this partially ionized gas differ markedly from those of an

ordinary gas. There are now several collision cross sections which have to be considered: those for atoms against atoms, atoms against ions, and atoms against electrons. Equation (18) now becomes

$$\eta = \frac{1}{3} \sum_j n_j m_j \lambda_j \bar{v}_j, \quad (19)$$

where  $j$  refers to atoms, ions, and electrons. The mean free path for, say, the atoms in this situation is given as

$$\lambda_a = \frac{1}{n_a Q_a^a + n_i Q_i^a + n_e Q_e^a}. \quad (20)$$

It will be noted that now the factor  $n_i$  does not cancel, and a pressure-dependent form of  $\eta$  is obtained. This is essentially a result of the fact that in general the ionization equilibrium depends on the pressure.

Expanding Eq. (19), we obtain for the viscosity

$$\eta = \frac{n_a m_a \bar{v}_a}{3 (n_a Q_a^a + n_i Q_i^a + n_e Q_e^a)} + \frac{n_i m_i \bar{v}_i}{3 (n_i Q_i^i + n_a Q_a^i + n_e Q_e^i)} + \frac{n_e m_e \bar{v}_e}{3 (n_e Q_e^e + n_i Q_i^e + n_a Q_a^e)}. \quad (21)$$

Here again, the subscripts  $a$ ,  $e$ , and  $i$  refer to atoms, electrons, and ions, respectively. The last term in this equation can be neglected since the product  $(m \cdot v)$  for electrons is small compared to that for the atoms or ions. In evaluating this equation, we take values for the

atom-atom cross sections from the literature [3, 28, 29] which have been estimated on the basis of kinetic theory. Further, we assume here that  $Q_a^e \approx Q_a^i$ . Values for the viscosity obtained in this manner for argon and nitrogen are given in Table 2 along with values previously calculated using theoretically estimated values for all of the cross sections. A value for  $\eta$  of  $26.9 \times 10^{-4}$  gm/cm-sec is computed for helium at 15,000°K on the basis of this work and can be compared with a value of  $41.0 \times 10^{-4}$  gm/cm-sec given in [29]. In general, the values obtained here are some 30 to 50 per cent lower than previously estimated and seem to be approaching a minimum near 2 ev, where the atom-electron collision cross sections are the highest.

The electrical conductivity, another transport property which was obtained by current density and electric field strength measurements, is shown for argon and nitrogen in Figures 26 and 27. A value of  $\sigma = .65 \times 10^{13}$  esu was obtained for helium at 15,000°K. No direct comparison was made for this parameter with previous estimates. Considering the over-all experiment, it is felt that an accuracy of  $\pm 15\%$  may be attached to any of the figures given in this report. The largest single source of error may be expected to lie with the spectroscopic temperature measurements, which involve spectral plate calibration and other standard data reduction techniques.

Correlation of these properties and others is being continued for argon, helium, and nitrogen. Further, future experiments are expected to yield experimental data for hydrogen, krypton, and xenon, and this information will also be compared with data available in the literature.

Table 2. Viscosities for Argon and Nitrogen

$10^4 \eta$ , g/cm-sec

Temperature °K	Argon		Nitrogen	
	Computed on Basis of Present Experiments	Ref. 29 Values	Computed on Basis of Present Experiments	Ref. 28 Values
10,000	20.1	31.0	----	21.2
12,000	18.5	35.5	19.4	22.6
14,000	17.3	39.8	14.3	19.5
16,000	16.0	----	3.8	----
18,000	14.8	----	0.90	----

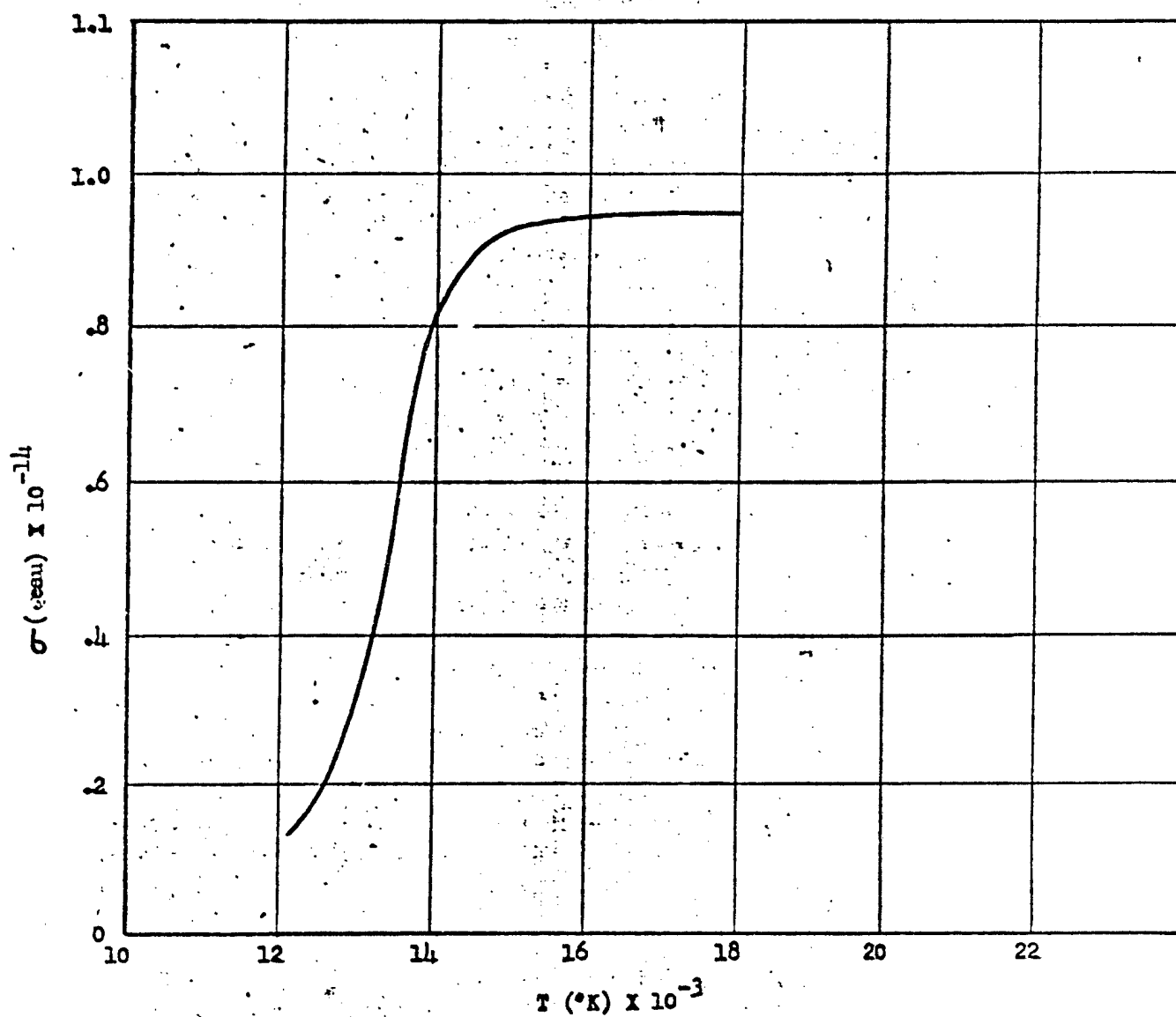


FIG. 26 ELECTRICAL CONDUCTIVITY vs TEMPERATURE FOR ARGON

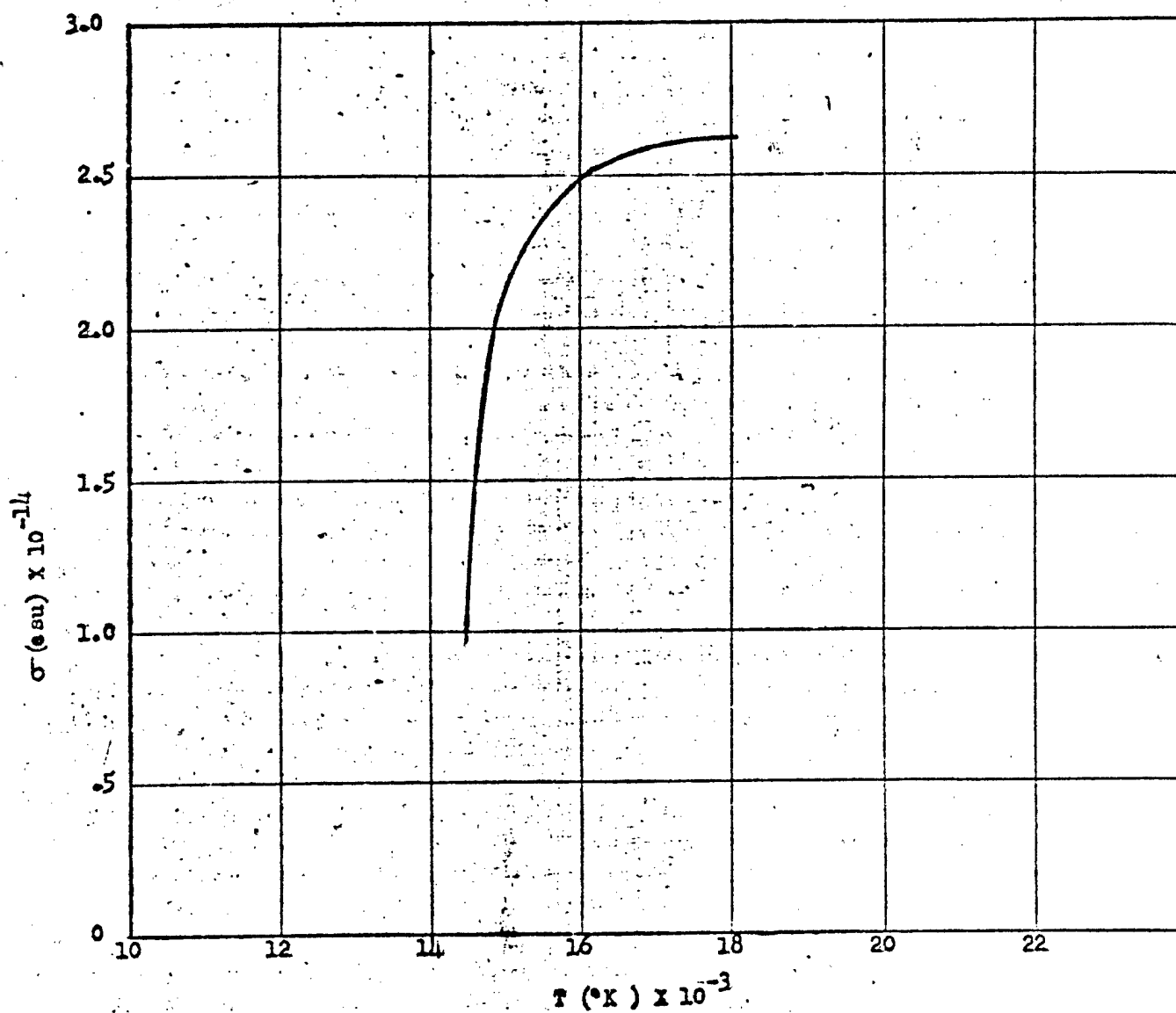


FIG. 27 ELECTRICAL CONDUCTIVITY vs TEMPERATURE FOR NITROGEN

#### 4. BIBLIOGRAPHY

1. Griem, H. R., Plasma Spectroscopy, Proceedings of Fifth International Conference on Ionization Phenomena in Gases, Munich, 1961.
2. Finkelberg, W., and Maecker, H., Handbuch der Physik, Vol. 22, (Springer Verlag Berlin) 1956.
3. Lochte-Holtgreven, W., Reports on Progress in Physics, 21, 312 (1958).
4. Lenard, P., Ann. der Physik, 12, 714 (1903).
5. Ramsauer, C., Ann. der Physik, 64, 513 (1921).
6. Mayer, H. F., Ann. der Physik, 64, 451 (1921).
7. Brown, S. C., Basic Data of Plasma Physics, John Wiley & Sons, 1959.
8. Olsen, H. N., Phys. Fluids, 2, 614 (1959).
9. Barr, T. A., and Cason, C., Quarterly Research Reviews, Army Rocket and Guided Missile Agency Report No. TN 1C1N-23, 1960.
10. Cason, C., and Smith, C. R., Quarterly Research Reviews, Army Rocket and Guided Missile Agency Report No. TN 1C1N-25, 1960.
11. Burhorn, F., and Wienicke, R., Zeitschr. für Physikalische chemie, 215, 269 (1960).
12. Spitzer, L., and Härm, R., Phys. Rev., 80, 230 (1950).
13. Spitzer, L., and Härm, R., Phys. Rev., 89, 977 (1953).
14. Gvosdover, S. D., Phys. Z. Sovjet, 12, 164 (1937).
15. Maecker, H., Peters, Th., and Schenk, H., Zeit. für Physik, 40, 119 (1955).

16. Optical Spectrometric Measurements of High Temperatures, Edited by P. J. Dickerman, University of Chicago Press, 1961.
17. Olsen, H. N., Private Communication.
18. Johnson, W. B., Private Communication.
19. Hattenberg, A. T., Dissertation, University of Maryland, 1961.
20. Richter, J., Zeits. für Astrophysik, 51, 177 (1961).
21. Nestor, O. H., S.I.A.M. Review, 2, 200 (1960).
22. Griem, H. R., Baranger, M., Kolb, A. C., and Oertel, G., Neutral Helium Lines (To be published).
23. Berg, H., Dissertation, University of Maryland, 1961.
24. Olsen, H. N., Proceedings of the 12th Gaseous Electronics Conference, NBS, 1959.
25. Gericke, W. E., Zeits. für Astrophysik, 53, 68 (1961).
26. Mower, L., Phys. Rev. 89, 947 (1953).
27. Massey, H. S. W., and Morseiwitsch, B. L., Proc. Roy. Soc., A205, 483 (1951).
28. Hansen, C. F., NACA Report TN 4150, 1958.
29. Amdur, L., and Mason, E. A., Phys. Fluids, 1, 370 (1958).